Convergence acceleration in scattering series and seismic waveform inversion using nonlinear Shanks transformation

---

A Dissertation Presented to

The Faculty of the Department of Physics

University of Houston

In Partial Fulfillment

of the Requirements for the Degree

Doctor of Philosophy

By

Roya Eftekhar

May 2018

Convergence acceleration in scattering series and seismic waveform inversion using nonlinear Shanks transformation

Roya Eftekhar

APPROVED:

Dr. Yingcai Zheng, Chairman

Dr. Liming Li

Dr. Gemunu. H. Gunarantne

Dr. Shoujun Xu

Dr. Lowell.Wood

Dean, College of Natural Sciences and Mathematics

ACKNOWLEDGMENTS

I have been fortunate to pursue my PhD study in Dr. Yingcai Zheng's group at University of Houston. During the past four years, I have received a lot of help and encouragements. My deepest gratitude is to my advisor Dr. Yingcai Zheng for his inspired instruction and continuous support during my PhD study and research. What I have learned from him not only benefits my research projects, but also my life and future career. I will always appreciate his support and guidance through my study at UH. I would also appreciate the invaluable help of Dr. Hao Hu who always gave me all of his support to have better understanding of my research; I really learned many things in this field from him, I always received his encouragement and help in all aspects of my research. He was always available to answer every single of my question immediately in the most professional way. He taught me how to pay attention to details and the correct way of thinking about my research.

I would also like to thank Dr. Kevin E Bassler, Dr. Liming Li, Dr. Gemunu. H. Gunarantne, Dr. Lowell Wood, and Dr. Shoujun Xu for their time and serving as members of my dissertation committee.

Furthermore, I would like to thank Dr. Wu-Pei Su for introducing me to Dr. Liming Li as my co-advisor in my PhD program. Also I have a spatial thank to Dr.

Liming Li who accepted not only to be in my dissertation committee but also as my co-advisor during my PhD program.

I respectfully thank Dr. Gemunu H. Gunarantne for all of his support to make this journey possible for me to work with Dr. Zheng.

I would like to thank Dr. Ming Zhang who has been supportive during my research. Without his encouragement and his scientific suggestion, it would not be possible to finish this hard journey. He always supported me how to stay strong even when I was disappointed, I could benefit his knowledge and continuous help to improve my study.

I would like to thank Dr. Mojdeh Niazmand for giving me her various forms of help and support. I am also thankful to Dr. Arthur Weglein, Dr. Kristopher Innanen, for their help and giving good suggestions in my study.

I am also grateful to Naomi Haynes, for all of her help and assistance during my study at the Physics Department.

Finally, I would also like to express my deepest gratitude to my parents for their constant love, concern, and support. They were always there for me, caring about me and encouraging me. None of this would have been possible without the support of my parents.

Convergence acceleration in scattering series and seismic waveform inversion using nonlinear Shanks transformation

---

An Abstract of a Dissertation

Presented to

the Faculty of the Department Physics

University of Houston

In Partial Fulfillment

of the Requirements for the Degree

Doctor of Philosophy

By

Roya Eftekhar

May 2018

ABSTRACT

An iterative solution process is fundamental in seismic inversion, such as in full-waveform inversions and inverse scattering methods. However, the convergence process could be slow or even divergent depending on the initial model used in the iteration. We propose to apply Shanks transformation (ST for short) to accelerate the convergence of the iterative solution. ST is a local nonlinear transformation, which transforms a series locally into another series with improved convergence property. ST separates the smooth background trend called the secular term versus the oscillatory transient term and then accelerates the convergence of the secular term. Because the transformation is local, we do not need to know all the terms in the original series and this is very important in the numerical application of ST. I propose to apply the ST in the context of both the forward Born series and the inverse scattering series (ISS). I test the performance of the ST in accelerating the convergence using several numerical examples, including three examples of forward modeling using the Born series and two examples of velocity inversion based on ISS. We observe that ST is very helpful in accelerating the convergence and it can achieve convergence even for a weakly divergent scattering series. As such, it provides us a useful technique to invert for a large-contrast medium perturbation in seismic inversion. The method developed in this dissertation can also be used in other fields such as in electromagnetics, quantum mechanics, and possibility medical imaging.

CONTENTS

ACKNOWLEDGMENTS ..... **iii**

ABSTRACT ..... **vi**

CONTENTS ..... **vii**

LIST OF FIGURES ..... **x**

Chapter 1 Introduction and background **1**

1.1 Challenges in waveform inversion in seismic exploration 1

1.2 Proposed solution: Convergence acceleration using Shanks transform 3

1.3 Dissertation structure 5

1.4 Impact of the thesis work 8

Chapter 2 Introduction of Shanks Transformation **9**

2.1 Introduction 9

2.2 Shanks Transformation 9

2.3 Application of Shanks transformation for an infinite series 11

2.4 Taylor series and its Shanks transformation 13

2.5 Summary on Shanks transform 14

Chapter 3 Forward scattering series and its Shanks transformation 16

3.1 Introduction 16

3.2 The Born series and its Shanks transformation 18

3.3 Benchmark modeling using propagator matrix method 20

3.4 Numerical examples 22

3.5 Application of ST on a convergent Born series 23

3.6 Application of ST on a slowly convergent Born series 30

3.7 Application of ST on a divergent Born series 36

3.8 Summary 41

Chapter 4 Inverse scattering and Shanks Transformation 42

4.1 Background of seismic exploration 42

4.2 Inverse scattering series introduction 46

4.3 Numerical example 50

4.3.1 Three-layered velocity model 50

4.3.2 Seven-layered velocity model 59

Chapter 5 Conclusions and future work 66

REFERENCES **68**

APPENDICES **76**

A. Forward modeling using the Born series 76

B. Derivation of reflection and transmission coefficient from PM method 79

C. Velocity inversion from inverse scattering series 83

LIST OF FIGURES

Figure 1. Different orders of shanks transformation. The first column corresponds to the number of terms used (n). The second column is (A_n). The third column corresponds to the sequences from *1st* order $\{S_n^1\}$ of ST after applying on (A_n). The fourth and the fifth columns are the *2nd* and *3rd* orders ST, respectively. 12

Figure 2. Convergence for different orders of ST. Comparison of $A_n(z)$ with its *1st; 2nd* and *3rd* orders ST. 14

Figure 3. Reflected and transmitted waves in the medium. The terms $e^{ik_0 z}$ and $\mathrm{R}e^{-ik_0 z}$ are the incident and reflected waves respectively in the reference medium. $A_1 e^{ik'z}$ and $A_2 e^{-ik'z}$ are waves in the second layer (anomaly) and the $Te^{ik_0 z}$ is the transmitted wave in the reference medium. 21

Figure 4. Three- layered velocity model, source and receiver are deployed at depth 0 km and 15 km, marked by the red star and blue triangle, respectively. 25

Figure 5. The sequence of complex-valued wavefield of the fast convergent $\{P_n\}$ at 0.1 Hz. Blue and red lines with circles corresponds to the real and imaginary parts of $\{P_n\}$ respectively..... 26

Figure 6. Comparison of complex-valued wavefield of $\{P_n\}$ with and without ST at 0.1 Hz. Blue and red lines with circles correspond to the real and imaginary parts of $\{P_n\}$ (denoted as "Born Re" and "Born Im" in the legend), respectively. Black circles correspond to the real and imaginary parts of $\{S_n^1[P_n]\}$ (denoted as "Shanks Re" and "Shanks Im" in the legend), respectively..... 27

Figure 7. Comparison of the theoretical wavefield calculated by PM method and the *6-th* term of the *1st* order ST of the Born wavefield and the *6-th* term of the Born wavefield without ST. Blue and red solid lines correspond to the real and imaginary parts of theoretical wavefield (denoted as "PM Re" and "PM Im" in the legend), respectively. Blue and red circles correspond to the real and imaginary parts of the *6-th* term of the *1st* order ST of the Born wavefield. Green and purple lines correspond to the real and imaginary parts of the *6-th* term of the Born wavefield without ST..... 28

Figure 8. Comparison of the theoretical wavefield calculated by PM method and the *6-th* term of the *1st* order ST of the Born wavefield. Blue and red solid lines correspond to the real and imaginary parts of theoretical wavefield (denoted as "PM Re" and "PM Im" in the legend), respectively. Blue and red circles correspond to the real and imaginary parts of the *6-th* term of the first order ST of the Born wavefield..... 29

Figure 9. One-dimensional model with three interfaces. The source and receiver are deployed at x=0 and x=15 the red star and blue triangle illustrate source and receiver respectively. This model is the same as the model shown in Figure 4. 31

Figure 10. The sequence of complex-valued wavefield of the slowly convergent $\{P_n\}$ at 0.14 Hz. Blue and red lines with circles corresponds to the real and imaginary parts of $\{P_n\}$, respectively..... 32

Figure 11. Comparison of the complex-valued Born wavefield P_n and its *3*rd order ST at 0.14 Hz for the model in Figure 9. Blue and red lines with circles correspond to the real and imaginary parts of P_n , respectively. Black circle corresponds to the real and imaginary parts of $\{S_n^3[P_n]\}$, respectively..... 33

Figure 12. Comparison of the theoretical wavefield calculated by PM method, the *8-th* term of the *3*rd ST of the Born wavefield and *8-th* term of Born wavefield without ST. Blue and red solid lines correspond to the real and imaginary parts of theoretical wavefield, respectively. Blue and red circles correspond to the real and imaginary parts of the *8-th* term of the *3*rd order ST of the Born wavefield. Green and purple lines correspond to the real and imaginary parts of the *8-th* term of the Born wavefield without ST..... 34

Figure 13. Comparison of the theoretical wavefield calculated by PM method and the *20-th* term of the 3rd order ST of the Born wavefield. Blue and red solid lines correspond to the real and imaginary parts of theoretical wavefield, respectively. Blue and red circles correspond to the real and imaginary parts of the *20-th* term of 3rd order ST of the Born wavefield. 35

Figure 14. Three-layered model with source (star) and receiver (triangle) located at depth 0 m and 1100 m, respectively. The thickness of anomaly of this model is 120 m. 37

Figure 15. Complex valued of divergent wavefield of P_n .Blue and red lines with circles correspond to the real and imaginary parts of P_n respectively. 38

Figure 16. Comparison of the theoretical depth wavefield using PM and the divergent Born wavefield at the *10-th* term. Blue and red lines show the real and imaginary parts of the theoretical wavefield, respectively. Green and purple lines correspond to the real and imaginary parts of the divergent Born wavefield, respectively. 39

Figure 17. Comparison of the PM wavefield and the *20-th* term of the 1st, 2nd and 3rd orders ST of the Born series. 40

Figure 18. Comparison of the theoretical wavefield using PM and the *20-th* term of the *5-th* order ST of the Born wavefield. 41

Figure 19. Example of marine case: source (star) and receivers (triangles) are located within the water column. Energy arrivals produced by a single reflection are called primaries. Energy arrivals produced by multiple reverberations are called multiples (From Ramirez (2007)). 45

Figure 20: A three-layered velocity model (two interfaces) with both the source (red star) and receiver (blue triangle) deployed on the surface with depth at 0 m. The high-velocity layer (1.4 km/s) has 40% of higher velocity than the reference velocity (1 km/s)..... 52

Figure 21. The observed waveform by the receiver at surface (depth at 0 m). The source wavelet is a Gaussian wavelet with a width of 1 s. There are two reflections from the *1st* and *2nd* interfaces and one internal multiples bounced between those two interfaces..... 53

Figure 22. Inverted velocity models based on the ISS (c_n) for the three-layered model (Figure 20) at the (a) *1st*, (b) *2nd*, iteration (without ST), respectively. ... 54

Figure 23. Inverted velocity models based on the ISS (c_n) for the three-layered model (Figure 20) at the (c) *10-th*, (d) *30-th*, iteration (without ST), respectively..... 55

Figure 24. Comparison of the inverted velocity model using ISS with *1st* order of ST at *10-th* iteration (red line) and inverted velocity model without ST at *30-th* iteration (blue line). 56

Figure 25. Comparison of the observed waveform (black line) and the modeled waveform using the inverted velocity with the *1st* order ST at *10-th* term. The modeled waveform matches the observed waveform well. 57

Figure 26. The convergences of the waveform residual between the observed and the modeled waveform. The black line and blue line represent the waveform residual without ST and with the *1st* order ST, respectively. 58

Figure 27. A seven-layered velocity model (6 interfaces) with the source and receiver on the surface at depth 0 m. There are three high-velocity layers and two low-velocity layers with different velocities and thicknesses embedded in the reference medium. 60

Figure 28. The observed waveform by the receiver at surface. The source wavelet is a Gaussian wavelet with a width of 1 s. There are six reflections from the *1st* to the *6-th* interfaces and several internal multiples bounced between those interfaces. 61

Figure 29. Inverted velocities based on the ISS (c_n) for the seven-layered model (Figure 27) t the (a) *1st*, and (b) *2nd*, iteration, respectively. Blue lines show the inverted velocity model c_n and black lines show the true velocity. 62

Figure 30. Inverted velocities based on the ISS (c_n) for the seven-layered model (Figure 27) at the (c) *7-th* and (d) *12-th* iteration, respectively. Blue lines show the inverted velocity model c_n and black lines show the true velocity.... 63

Figure 31. Comparison of the inverted velocity model without ST at the *12-th* iteration (blue line) and the inverted model at *7-th* term of the first order ST (red line). 64

Figure 32. Comparison of the observed waveform (black line) and the modeled waveform using the inverted model (red line) using the inverted velocity at 7-*th* term of the *1st* order ST. The modeled waveform well matches the observed waveform for both primary reflections and multiples. 65

Chapter 1

Introduction and background

In this Chapter, I will briefly discuss about the general seismic exploration including the forward scattering series (using the Born series), inverse scattering series (ISS), and also applying the Shanks transformation (ST for short) on the both forward and inverse scattering series. An overview of the dissertation is provided at the end of this chapter.

1.1 Challenges in waveform inversion in seismic exploration

Seismic waves are commonly used to investigate the Earth's interior structures and properties. Using the seismic data recorded by receivers, we can estimate the subsurface structure of earth using various kinds of waveform inversion methods (e.g., Tarantola 2005). Seismic waves are commonly used to remotely investigate the Earth's interior structure and properties. In seismic waveform inversion (e.g., Tarantola 2005, Tarantola 1984), the goal is to find a subsurface model such that the data misfit, between the observed data and the modeled data using this model is

acceptable, measured by some norm. The functional dependence between the data misfit and the model misfit determines the inversion scheme and such dependence is nonlinear (Wu and Zheng 2014). The nonlinear inversion problem is usually linearized and the true model could be readily obtained when the initial model and the true model is close. Seismic full waveform inversion of the Earth interior structure usually is a nonlinear inverse problem that is challenging to solve. The scattering theory is the basis to tackle this difficulty. The scattering theory describes seismic wave interaction with structures (e.g., Wu and Aki 1988, Weglein et al. 2003, Taylor 2012, Newton 2013, Zuberi and Alkhalifah 2014a, b, Alkhalifah 2010). Using the scattered wavefield, we can invert for structure. Traditionally, the nonlinear inversion problem is usually linearized using the single-scattering approximation and the correct model could be obtained when the perturbation between the initial model and the true model is weak (Weglein et al. 2003, Cohen and Bleistein 1977, Stolt and Weglein 1985). In the scattering theory, the wavefield in an inhomogeneous medium can be represented as a perturbation wavefield plus a reference wavefield. The wavefield satisfies the Lippmann-Schwinger equation that can be expanded to generate an infinite series called the scattering series. One fundamental type of series is the Born series (Matson 1996). In seismic forward modeling, the Born series is known to be divergent in general for large-scale strong perturbations (Wu 1994). Sams and Kouri (1969) solved

this problem by converting the Fredholm integral into a Volterra form (see also Yao et al. 2016) and proved the absolute convergence with arbitrary perturbation strength of the medium. However, for the inverse scattering series (ISS), Weglein et al. (1997) proposed to use the sub series approach to accomplish certain seismic tasks using the Fredholm form. The ISS can be used in to predict internal multiples, perform depth imaging and velocity inversion (Wang and Hung 2014, Arthur B. Weglein et al. 2012, Luo et al. 2011, Weglein et al. 2009, Weglein 2013, 2017). Using the Volterra form of the Lippmann-Schwinger equation, Yao et al. (2014b) proposed the Volterra inverse scattering series (VISS) formulation, but it still suffered the convergence issue (Yao et al. 2014a, Chou, Yao, and Kouri 2017, Yao et al. 2014b). To solve this divergence problem, Yao et al. (2014b) proposed to use the Cesàro summation to accelerate the VISS but with limited success.

1.2 Proposed solution: Convergence acceleration using Shanks transform

In this dissertation, I consider the convergence problem for both the Born series in the forward modeling and the inverse scattering series (ISS for short). The goal of forward modeling using the Born series is to model the wavefield excited by a source and propagated in an inhomogeneous model represented by a reference medium and

scatters. ISS is to estimate the velocity structure from the observed waveform data with an initial velocity model. Both the forward Born series and the ISS are nonlinear processes with respect to model parameters where the solution takes the form of an infinite series.

I propose to employ the Shanks transformation (ST), proposed by Shanks (1955), to accelerate the convergence of scattering series. ST is a nonlinear transformation, which transforms one sequence into another sequence with improved convergence properties. ST has been studied to accelerate the convergence of slow convergent sequences and even divergent sequences (e.g., Weniger 1989, Smith and Ford 1979, Levin 1972, Shanks 1955, Brezinski 1982). In many fields, ST was adopted to improve the series convergence in the calculation of electromagnetic Green's function in periodic structures (e.g., Singh et al. 1990, Singh and Singh 1991, Erricolo 2003) and the computational chemeical and physical studies (e.g., Weniger, Grotendorst, and Steinborn 1985, Grotendorst and Steinborn 1986). In seismic studies, ST has not been widely used except in a few cases where the ST was used to solve the dispersion equation in anisotropy media and optimize the wavefield extrapolation (e.g., Alkhalifah 2000, Stovas and Alkhalifah 2012, Alkhalifah 2013b, a). Here, I propose to apply ST on both the forward and inverse problems. I first revise the theory of ST and the applications of ST on the forward modeling using the Born series and velocity

inversion based on the ISS. Then I show the performance of these two applications of ST by several numerical examples. In this dissertation, I consider the convergence problem for both the Born series in forward modeling and the inverse scattering series (ISS for short) in the velocity inversion.

The goal of forward modeling using the Born series is to model the wavefield excited by a source and propagated in an inhomogeneous model constructed by a reference media and scatters. The velocity inversion based on the ISS is to estimate the velocity structure from the observed waveform data with an initial velocity model. Both the forward scattering series and the ISS are nonlinear processes where the solution takes the form of an infinite series.

1.3 Dissertation structure

This dissertation investigates several examples of applying the ST on the forward scattering series and inverse scattering.

In the forward scattering series, our goal is to calculate the wavefield in an inhomogeneous medium based on the Lippmann-Schwinger equation. This equation can be expanded into an infinite series called the Born series. This series is a nonlinear series in which its convergence process could be slow or even divergent. The radius of

convergence of the Born series depends on the initial model used in the iteration and perturbation. Applying ST on the Born series can accelerate the rate of convergence in summing up the series.

In the inverse scattering (IS), our goal is to find the velocity of the Earth's subsurface using recorded data on the Earth surface. Inverse scattering is a nonlinear process where the solution can also take the form of an infinite series called inverse scattering series (ISS). From ISS iterations to be discussed in this dissertation, we can calculate the model perturbation with respect to some known reference model. Once we obtain the model perturbation via ISS, we can recover the velocity based on the reference velocity (known). Usually, the model perturbation is solved in an iterative fashion. When a sequence of the velocity models are available, we can apply ST on this sequence (like in a series) to accelerate the solution process.

This dissertation is divided in to five chapters. The following gives a snapshot of the content in each chapter.

Chapter 1 (this chapter) gives an introduction and background review of seismic exploration. The problem of determining Earth material properties from seismic reflection data is an inverse scattering problem.

In Chapter 2, I introduce the Shanks transformation and its properties. In this chapter I will show the capability of the ST on improving the rate of convergence of

some series through examples. These examples can help us gain intuitive understanding of ST.

Chapter 3 discusses about the forward modeling using the Born series. Before we solve the inverse problem, we need to gain insight from modeling the forward series. In this chapter, three modeling examples using the Born series will be discussed. These examples include rapidly convergent, slowly convergent, and divergent Born series. I show that ST can be effective to speed up the convergence on these three different types of series.

Chapter 4 discusses about the inverse scattering series (ISS). Using only reflected waveforms recorded on the surface, we can recover medium properties of a layered medium. Most seismic imaging uses only primary reflection where the wave interacts with the layer interfaces/boundaries once. Waves that have interacted with boundaries more than once are called multiples. Multiple data is usually considered as noise. In this chapter, I use all types of data (primary & multiple) in the inverse scattering. Because removal of the multiple is a daunting task, the approach in Chapter 4 is very attractive in real applications. In this chapter, I will show examples using different layered models. We can see after applying ST on these examples, the convergence of inverse series is more rapid than the convergence without ST.

Chapter 5 provides the conclusions and findings of this dissertation.

1.4 Impact of the thesis work

In this dissertation, I am mainly concerned with the forward and inverse scattering problems in the context of one-dimensional layered media. Two- and three-dimensional media are not considered explicitly.

In spite of this limitation, the proposed approach can be immediately useful for imaging the tight oil/gas reservoirs because the geological layering in these unconventional settings is mostly horizontally layered.

Furthermore, there is no need to remove the multiples in the data before applying the proposed approach to image the subsurface. This is an added benefit because in the traditional imaging one has to identify and remove the multiples in the data. Removal of the multiples can be a challenging task.

Chapter 2

Introduction of Shanks Transformation

2.1 Introduction

Scattering theory is a form of perturbation analysis that is used in both forward and inverse problems. If the perturbation is weak, the series converges rapidly and, summing first several terms can give a good approximation to the exact solution. However, when the perturbation is large, the series may converge slowly or even diverge. Shanks method can accelerate convergence of a series.

2.2 Shanks Transformation

The Shanks transformation is a nonlinear method to improve the convergence property of a sequence of partial sums (or any sequence). Suppose we want to sum up the following series $A = \sum_{k=0}^{\infty} u_k$, where u_k is the *k-th* term of scattered wave in the Born series in our study. The partial sum A_n can be represented as

$$A_n = \sum_{k=0}^{n} u_k \tag{2.1}$$

A_n will approach to the limit A when $n \to \infty$ if the series is convergent. As shown by Bender and Orszag (1978), the *n-th* term in the sequence can take an asymptotic form when *n* is large

$$A_n = A + \alpha q^n . \tag{2.2}$$

Here αq^n is the transient part which fluctuates around the limit value A and α is a constant. We can use three terms, $A_{n-1} = A + \alpha q^{n-1}, A_n = A + \alpha q^n$ and $A_{n+1} = A + \alpha q^{n+1}$ to estimate A in equation (2.2). The ST of the sequence $\{A_n\}$, is a nonlinear local transformation represented as (Shanks 1955):

$$S_n^{\,1}[\{A_{0\le k\le n+1}\}] = \frac{A_{n+1}A_{n-1} - (A_n)^2}{A_{n+1} + A_{n-1} - 2A_n} , \tag{2.3}$$

where $\{S_n^{\,1}\}$ is the new sequence of ST which often converges faster than the original sequence $\{A_n\}$. The ST can be also applied again to the new sequence $\{S_n^{\,1}\}$ to obtain the second order ST, as $\{S_n^{\,2}\}$, to accelerate the convergence even further.

In this research, I propose the application of ST on different examples which will be discussed in this chapter and also in Chapters 3 and 4 on the Born series and the ISS.

2.3 Application of Shanks transformation for an infinite series

For a sequence $\left\{a_m\right\}$, the partial sum A_n (expanded form) is defined;

$$A_n = \sum_{m=0}^{n} a_m = a_0 + a_1 + a_2 + a_3 + \cdots + a_n \,. \tag{2.4}$$

The new sequence $\{A_n\}$ is defined as

$$\begin{aligned} A_1 &= a_0 \\ A_2 &= a_0 + a_1 \\ A_3 &= a_0 + a_1 + a_2 \\ A_4 &= a_0 + a_1 + a_2 + a_3 \\ &\vdots \\ A_n &= a_0 + a_1 + a_2 + a_3 + \ldots + a_{n-1} \end{aligned} \,. \tag{2.5}$$

n	A_n	1st shanks transformation $S_n^{\,1} = S(A_n)$	Second shanks transformation $S_n^{\,2} = S\{S(A_n)\}$	3rd shanks transformation $S_n^{\,3} = S[S\{S(A_n)\}]$
0	$A_0 = a_0$	-	-	-
1	$A_1 = a_0 + a_1$	$S_1^{\,1} = \frac{A_0A_2 - A_1^{\,2}}{A_0 + A_2 - 2A_1}$	-	-
2	$A_2 = a_0 + a_1 + a_2$	$S_2^{\,1} = \frac{A_1A_3 - A_2^{\,2}}{A_1 + A_3 - 2A_2}$	$S_1^{\,2} = \frac{S_1S_3 - S_2^{\,2}}{S_1 + S_3 - 2S_2}$	-
3	$A_3 = a_0 + a_1 + a_2 + a_3$	$S_3^{\,1} = \frac{A_2A_4 - A_3^{\,2}}{A_2 + A_4 - 2A_3}$	$S_2^{\,2} = \frac{S_2S_4 - S_3^{\,2}}{S_2 + S_4 - 2S_3}$	$S_1^{\,3}$
4	A_4 . .	$S_4^{\,1}$ . .	$S_3^{\,2} = \frac{S_3S_5 - S_4^{\,2}}{S_3 + S_5 - 2S_4}$	$S_2^{\,3}$
. .			$S_3^{\,2}$ . .	$S_3^{\,3}$
				$S_4^{\,3}$

Figure 1. Different orders of shanks transformation. The first column corresponds to the number of terms used (n). The second column is (A_n). The third column corresponds to the sequences from *1st* order $\{S_n^1\}$ of ST after applying on (A_n). The fourth and the fifth columns are the *2nd* and *3rd* orders ST, respectively.

2.4 Taylor series and its Shanks transformation

One of the slowly converging series is the Taylor series for the function:

$$A(z) = \frac{1}{(z+1)(z+2)}. \tag{2.6}$$

The *n-th* partial sum of the Taylor series is

$$\begin{aligned} A_n(z) &= \sum_{k=0}^{n} (-1)^n (1 - \frac{1}{2^{k+1}}) z^k \\ &= \frac{1}{(z+1)(z+2)} - \frac{(-z)^{n+1}}{z+1} + \frac{(-\frac{z}{2})^{n+1}}{z+2} \end{aligned} . \tag{2.7}$$

The poles of $A(z)$ at $z = -1$ and $z = -2$ affect the rate of convergence of $A_n(z)$ to $A(z)$. More than 1500 terms of this series are necessary to evaluate $A(0.99)$ accurate to 6 decimal places.

ST may be applied to the sequence (2.7). From numerical result of $A_n(z)$ and its ST shown in Figure 2, there is a considerable difference between the result of convergence driven without ST and after applying ST. Figure 2 represents the diagrams of sequence $\{A_n\}$ and its *1st*, *2nd* and *3rd* orders of ST. The sequence $\{A_n\}$ converges so slowly; however with applying several orders of ST, the rate of convergence will noticeably accelerate.

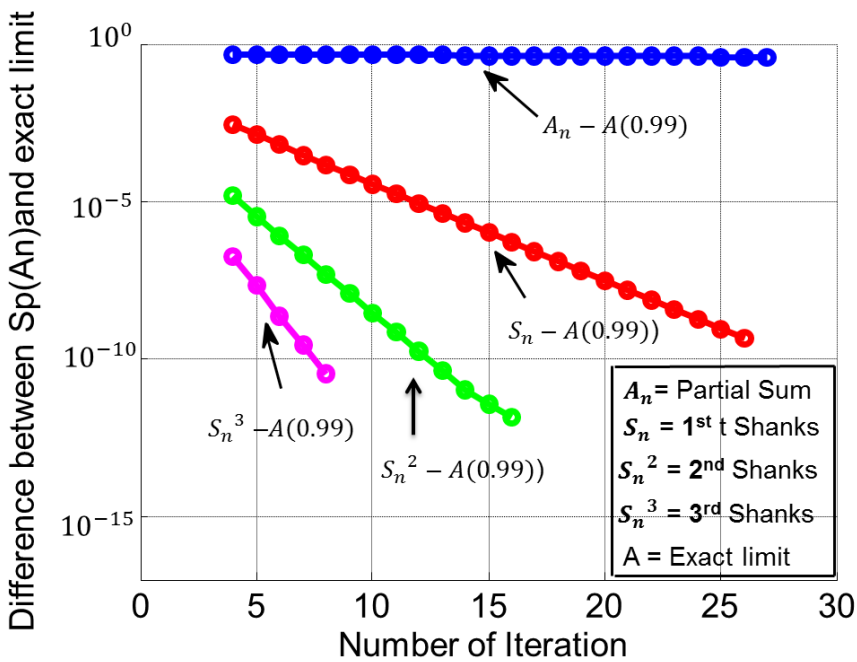

Figure 2. Convergence for different orders of ST. Comparison of $A_n(z)$ with its *1st; 2nd* and *3rd* orders ST.

2.5 Summary on Shanks transform

In this chapter, I have presented the introduction and definition of Shanks transformation theoretically and analytically. I also applied ST on a well-known Taylor series and showed the effect of this special transformation property to speed up

the convergence of that slowly convergent series. Ultimately I could approach the faster convergence of series in higher order of ST. In other words, convergence has been more rapid after applying ST on the series compare to the convergence of Taylor series without ST. This method is applicable to any sequence. Using higher order ST on the sequence, we can even get faster convergence with fewer terms. As an advantage of ST; since it is a local transformation, we do not need to know all terms of the series to compute ST.

Chapter 3

Forward scattering series and its Shanks transformation

3.1 Introduction

Scattering theory provides a theoretical framework to describe the seismic wave interaction with the medium. Using this approach, the wavefield in an inhomogeneous medium is represented as a perturbation field on a reference wavefield. This chapter introduces the forward Born scattering series. The goal of the forward problem is to calculate the wavefield which emanates from a localized source and propagates through a prescribed model. For simple models, the total wavefield contains various types of reflected and transmitted waves. I will show how scattering theory can be used to generate the same results.

Following the work of Weglein et al. (2003), I begin with the one dimensional (but with constant density) acoustic wave equation

$$[(\frac{\partial^2}{\partial z^2})-\left\{\frac{1}{c^2(z)}\right\}\left\{\frac{\partial^2}{\partial t^2}\right\}]G(z,z_s;t)=\delta(z-z_s)\delta(t)\,, \tag{3.1}$$

where the scalar $G(z, z_s; t)$ represents the Green's function at point z and time t due to a source at point z_s and time $t = 0$. The spatially varying velocity $c(z)$ can be characterized by a constant reference velocity c_0 and a perturbation $\alpha(z)$ so that

$$\frac{1}{c^2(z)} = \frac{1}{c_0^2}[1-\alpha(z)], \tag{3.2}$$

or

$$\alpha(z) = 1 - \frac{c_0^2}{c^2(z)}. \tag{3.3}$$

Fourier transforming equation (3.1) with respect to time and substituting equation (3.2) into equation (3.1) gives

$$[(\frac{\partial^2}{\partial z^2}) + (\frac{\omega^2}{c_0^2})]\tilde{G}(z, z_s; k) = \delta(z - z_s) + (\frac{\omega^2}{c_0^2})\alpha(z)\tilde{G}(z, z_s; k), \tag{3.4}$$

where $\tilde{G}$ is the Fourier transform of G with respect to $t, k_0 = \frac{\omega}{c_0}$ is the reference wavenumber, and ω is the temporal frequency. To find a solution to equation (3.4), consider the causal free space Green's function $\tilde{G}_0(z, z_s; k)$ which satisfies the equation

$$[(\frac{\partial^2}{\partial z^2}) + (k_0^2)]\tilde{G}_0(z, z_s; k_0) = \delta(z - z_s). \tag{3.5}$$

Using this Green's function as a reference wavefield, an integral equation corresponding to equation (3.4) and its physical boundary conditions (Weglein et al. 2003) leads us to derive the forward Born series in the following section.

3.2 The Born series and its Shanks transformation

For acoustic wave propagation in an inhomogeneous medium of constant density with source located at z_s and receiver located at z_g, the Green's function $G(z_g, \omega; z_s)$ in the frequency ω domain can be represented as the Lippmann-Schwinger equation (Clayton and Stolt 1981):

$$G\left(z_g, z_s, \omega\right) = G_0\left(z_g, z_s, \omega\right) + k_0^{\,2} \int_{-\infty}^{\infty} G_0\left(z_g, z', \omega\right) V\left(z'\right) G\left(z', z_s, \omega\right) dz', \tag{3.6}$$

where the scattering potential is defined with respect to the background velocity in an acoustic isotropic

$$V\left(z'\right) = \left[1 - \frac{c_0^2}{c^2\left(z'\right)}\right], \tag{3.7}$$

in which $k_0 = \omega / c_0$ is the wavenumber in the background (reference) medium. $c_0(z)$, and $c(z)$ are the reference velocity and the true velocity at depth z, respectively;

$G_0(z_g, \omega; z_s)$ is the Green's function in the reference velocity c_0 from the source z_s to the receiver z_g and $G(z_g, \omega; z_s)$ is the Green's function for the true medium $c(z)$.

We can also write equation (3.6) in symbolic form as (also see Appendix A)

$$\mathbf{G} = \mathbf{G_0} + \mathbf{G_0 V G}. \tag{3.8}$$

Here, operator $\mathbf{V}$ contains a k^2 term where $k = \frac{\omega}{c_0}$. Iterating equation (3.8) can generate a scattering series, called the Born series,

$$\underbrace{\mathbf{G}}_{P} = \underbrace{\mathbf{G_0}}_{p_0} + \underbrace{\mathbf{G_0 V G_0}}_{p_1} + \underbrace{\mathbf{G_0 V G_0 V G_0}}_{p_2} + \underbrace{\mathbf{G_0 V G_0 V G_0 V G_0}}_{p_3} + \cdots. \tag{3.9}$$

In an inhomogeneous medium, for a given source at z_s, the waveform recorded by the receiver at z_g, can be approximated with the *n-th* order of Born approximation, represented as:

$$P_n = \sum_{i=0}^{n-1} p_i, \tag{3.10}$$

where p_i is the *i-th* term of the Born series corresponding to the right hand side of equation (3.9).

After applying the ST on the sequence of $\{P_k\}$ we can obtain the first order ST:

$$S_n^{\,1}\left[\left\{P_{0\le k\le n+1}\right\}\right]=\frac{P_{n+1}P_{n-1}-(P_n)^2}{P_{n+1}+P_{n-1}-2P_n}\,, \tag{3.11}$$

where $S_n^{\,1}\left[\left\{P_{0\le k\le n+1}\right\}\right]$ represents the *n-th* term of the first order ST of the sequence $\{P_k\}$.

Furthermore, we can apply the ST on the new sequence $\left\{S_n^{\,1}\left[\left\{P_{0\le k\le n+1}\right\}\right]\right\}$ to obtain the second order ST form. To obtain the second order ST of P_k, we can implement the following:

$$S_n^{\,2}\left[\left\{P_{0\le k\le n+2}\right\}\right]=\frac{S_{n+1}^1S_{n-1}^1-(S_n^1)^2}{S_{n+1}^1+S_{n-1}^1-2S_n^1}\,. \tag{3.12}$$

Similarly, the *m-th* order ST can be obtained using the terms in the *(m-1)-th* order ST.

3.3 Benchmark modeling using propagator matrix method

Previously I mentioned that the acoustic wave equation and the wavefield can be obtained from the Born series. To benchmark the Born result, we use the propagating matrix (PM) method (Haskell 1953, Aki and Richards 2002) (see Appendix B). We

start with a simple three-layered model. In the Figure 3, an inhomogeneous medium located in a homogeneous medium.

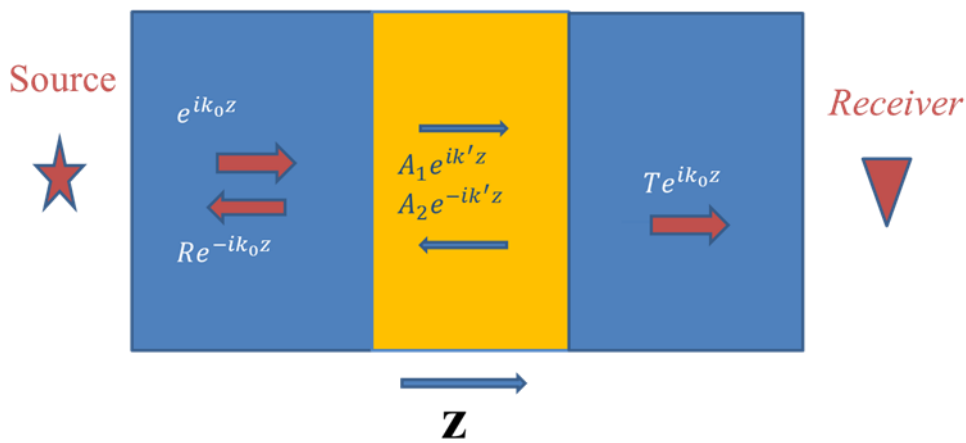

Figure 3. Reflected and transmitted waves in the medium. The terms e^{ik_0z} and Re^{-ik_0z} are the incident and reflected waves respectively in the reference medium. $A_1e^{ik'z}$ and $A_2e^{-ik'z}$ are waves in the second layer (anomaly) and the Te^{ik_0z} is the transmitted wave in the reference medium.

In the PM method (Figure 3), the wavefield in each layer can be written as

$$P_1 = e^{ik_0 z} + \mathrm{R}e^{-ik_0 z} \text{ in Layer 1,} \tag{3.13}$$

$$P_2 = A_1 e^{ik_1 z} + A_2\, \mathrm{e}^{-ik_1 z} \text{ in Layer 2,} \tag{3.14}$$

$$P_3 = Te^{ik_0 z} \text{ in Layer 3,} \tag{3.15}$$

where $k_0 = \frac{\omega}{c_0}$ and $k_1 = \frac{\omega}{c_1}$ are the wave numbers of the reference and anomaly layers respectively; c_0 and c_1 are velocities of reference and anomalous medium, respectively.

We need to find coefficients R, A_1, A_2 and T by ensuring boundary conditions. On each boundary, the pressure is continuous and the normal component of the particle velocity is continuous (see Appendix B). These boundary conditions allow us to find the coefficients. Once we get the reflection and transmission coefficients then we can calculate the total pressure wavefield.

3.4 Numerical examples

To demonstrate the ST performance in accelerating the convergence of the iterative process, we test ST on several examples in the context of forward modeling using the Born series and velocity inversion based on ISS. In those forward modeling examples,

first we apply ST on a model corresponding to the data with a frequency of 0.1 Hz. In this case, the size of anomaly is half of the wavelength in the reference medium and the Born series is supposed to converge rapidly. Then using the same model, we test ST at a higher frequency of 0.14 Hz and the anomaly-size-to-wavelength ratio is 0.7. In this case, the Born series converges slowly. In the third forward modeling example, we use another model with an anomaly size larger than the wavelength (anomaly-size-to-wavelength ratio as 1.2) where the Born series would diverge. For examples of velocity inversion based on the ISS, we first test the ST in recovering a simple three-layered velocity model and then apply the ST on a more complex velocity model with seven layers.

3.5 Application of ST on a convergent Born series

In the first example, we use a three-layered model (Figure 4). We set a low velocity layer (P-wave velocity as 0.75 km/s) with depth from 5 km to 10 km as the anomaly in a reference medium (1 km/s). We use the frequency at 0.1 Hz and the reference velocity of 1 km/s for calculating the Born waveform P_n recorded at the receiver using the Born series (Figure 5). The ratio anomaly-size-to-wavelength ratio is 0.5 (5 km anomaly-size and 10 km wavelength in the background medium). Then we apply the

ST on $\{P_n\}$ to construct the first-order ST of $\{P_n\}$, symbolized as $S_n^1[P_n]$. If the updates is less than 1% of the current term of series, we determinate the series has converged. In this case, $\{P_n\}$ (without ST) becomes convergent at the *35-th* term while $\{S_n^1[P_n]\}$ (with ST) converges at the *6-th* term (Figure 6). We can calculate the depth wavefield of P_n recorded by receivers at each depth, called as the Born wavefield. We construct the wavefield corresponding to the *6-th* term of the first order ST of the Born wavefield and the *6-th* term of Born wavefield without ST (Figure 7). We also calculated the theoretical complex-valued wavefield using the propagator matrix method at 0.1 Hz. The *6-th* term of the first order ST of the Born wavefield matches well with the theoretical wavefield both in the real and imaginary parts (Figure 8). The *6-th* term of the Born wavefield without ST is different with the theoretical wavefield. From this example, we can see that ST can accelerate the convergence of the Born series from the *35-th* term to the *6-th* term where the anomaly-size-to-wavelength ratio is 0.5.

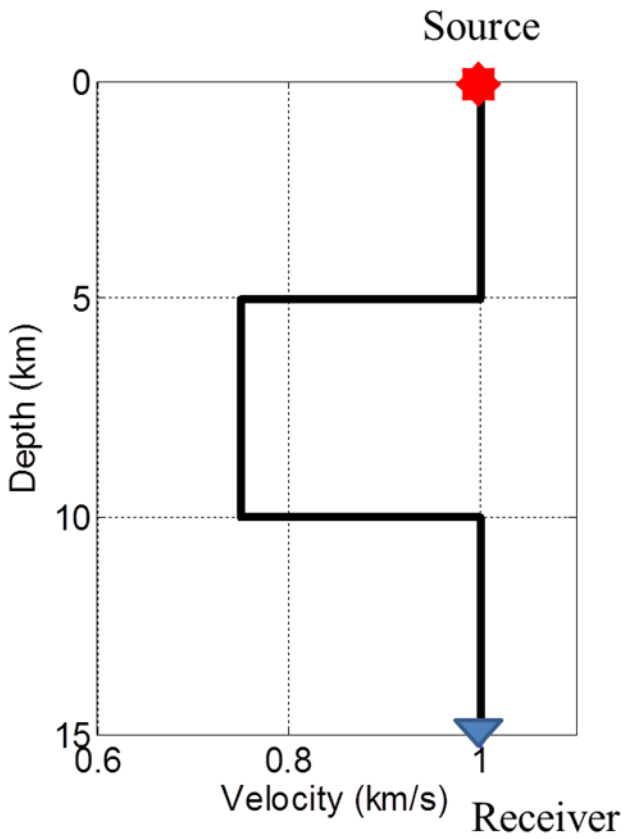

Figure 4. Three- layered velocity model, source and receiver are deployed at depth 0 km and 15 km, marked by the red star and blue triangle, respectively.

The fast convergence of the Born series is observed (Figure 5) at the low frequency 0.1 Hz. The convergence is reached after ~35 iterations both in real and imaginary parts.

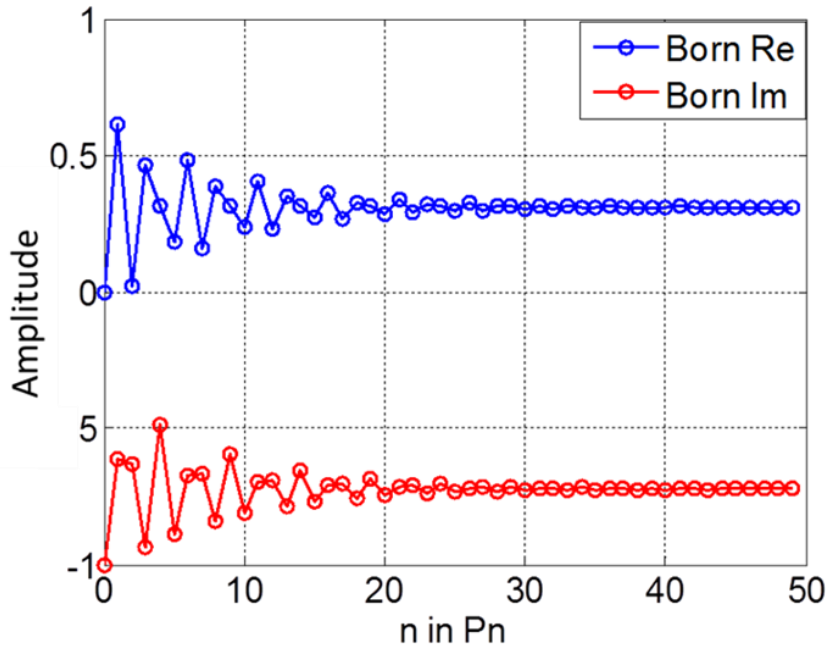

Figure 5. The sequence of complex-valued wavefield of the fast convergent $\{P_n\}$ at 0.1 Hz. Blue and red lines with circles corresponds to the real and imaginary parts of $\{P_n\}$ respectively.

In order to obtain convergence, we need about 35 iterations without ST for both real and imaginary part. After applying ST on the sequence of $\{P_n\}$ represented in Figure 6, the number of terms used to achieve convergence is reduced (Figure 6). In the first order ST, the sequence converges after three iterations.

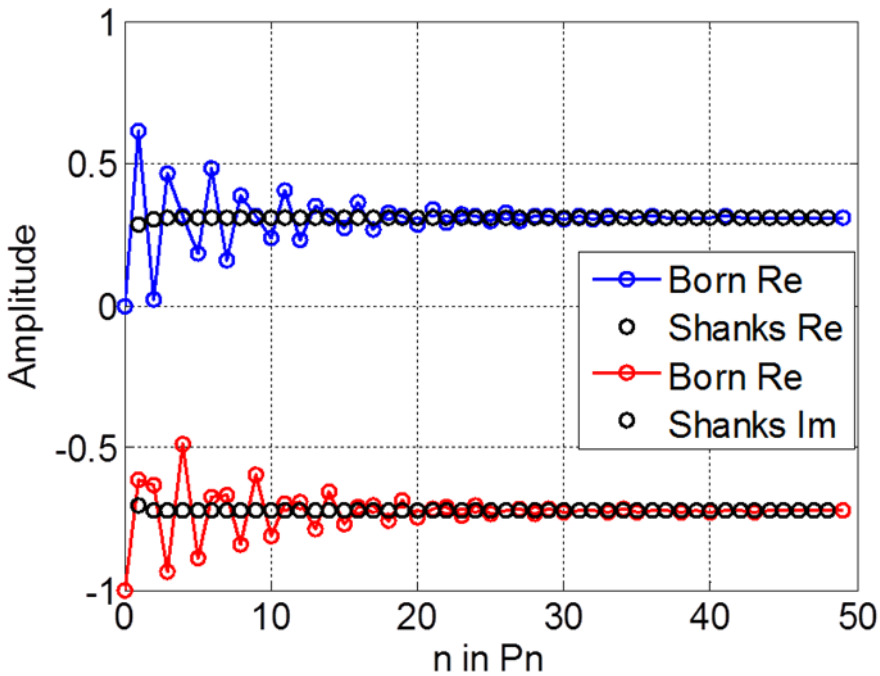

Figure 6. Comparison of complex-valued wavefield of $\{P_n\}$ with and without ST at 0.1 Hz. Blue and red lines with circles correspond to the real and imaginary parts of $\{P_n\}$ (denoted as "Born Re" and "Born Im" in the legend), respectively. Black circles correspond to the real and imaginary parts of $\{S_n^1[P_n]\}$ (denoted as "Shanks Re" and "Shanks Im" in the legend), respectively.

We can also place receivers at different depths in the model. In Figure 7, the real and imaginary parts of the *6-th* term of the Born wavefield without ST is still far from the theoretical wavefield (PM) while after applying ST, the Born wavefield will converge to the PM results. We focused the complete convergence consequence in Figure 8.

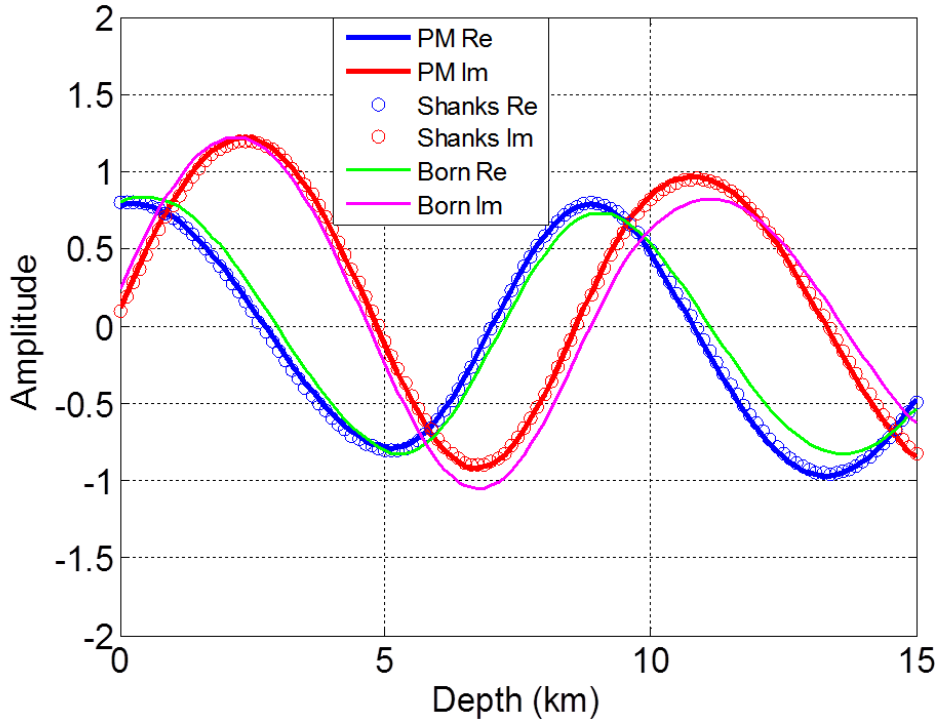

Figure 7. Comparison of the theoretical wavefield calculated by PM method and the *6-th* term of the *1*st order ST of the Born wavefield and the *6-th* term of the Born wavefield without ST. Blue and red solid lines correspond to the real and imaginary parts of theoretical wavefield (denoted as "PM Re" and "PM Im" in the legend), respectively. Blue and red circles correspond to the real and imaginary parts of the *6-th* term of the *1*st order ST of the Born wavefield. Green and purple lines correspond to the real and imaginary parts of the *6-th* term of the Born wavefield without ST.

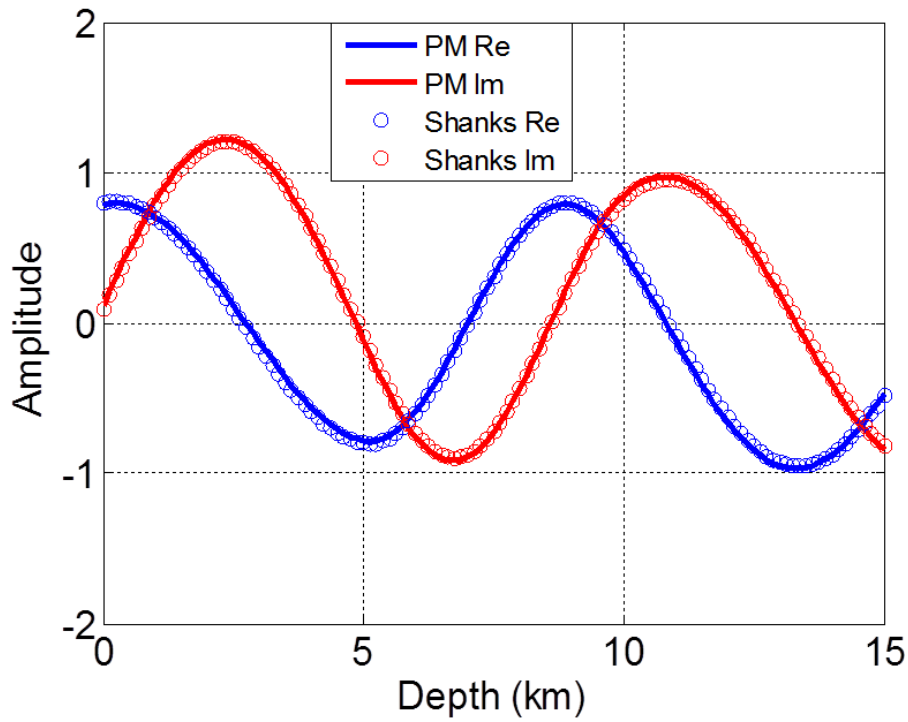

Figure 8. Comparison of the theoretical wavefield calculated by PM method and the *6-th* term of the 1st order ST of the Born wavefield. Blue and red solid lines correspond to the real and imaginary parts of theoretical wavefield (denoted as "PM Re" and "PM Im" in the legend), respectively. Blue and red circles correspond to the real and imaginary parts of the *6-th* term of the first order ST of the Born wavefield.

3.6 Application of ST on a slowly convergent Born series

In the second example, we use the same model as in the previous example (Figure 9). We changed the frequency from 0.1 Hz to 0.14 Hz to make the anomaly-size-to-wavelength ratio as 0.7. The Born waveform P_n converges slowly after about the *70-th* term (Figure 10) while its third order ST converges at only the *8-th* term (Figure 11). Similar to the previous example, we construct the *8-th* term of the third order ST of the Born wavefield and *8-th* term of the Born wavefield without ST. The Born wavefield without ST does not match with the theoretical wavefield by PM both in the real and imaginary parts (Figure 12) while the Born wavefield with ST matches well with the theoretical one both in real and imaginary parts (Figure 13). From this example, we can see that the ST is very helpful on accelerating the convergence of a slowly convergent Born series.

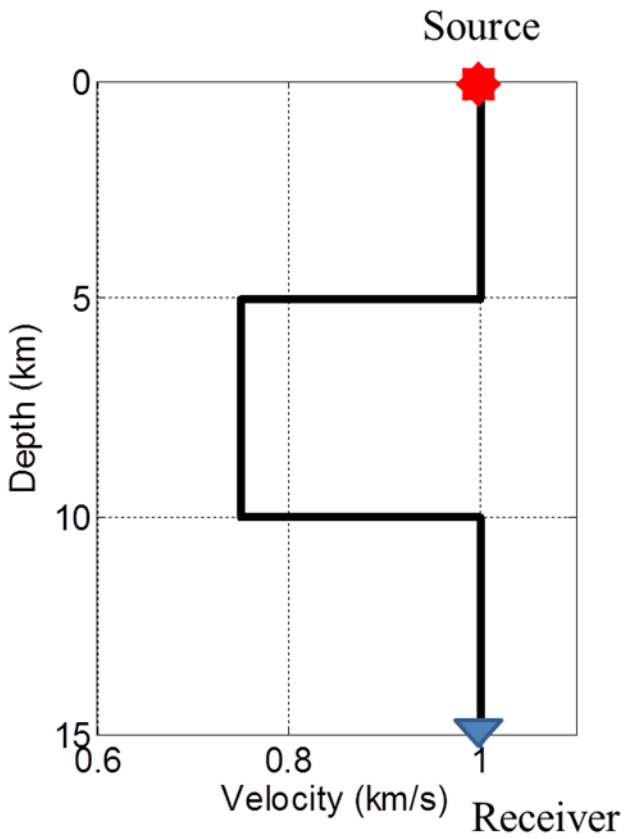

Figure 9. One-dimensional model with three interfaces. The source and receiver are deployed at x=0 and x=15 the red star and blue triangle illustrate source and receiver respectively. This model is the same as the model shown in Figure 4.

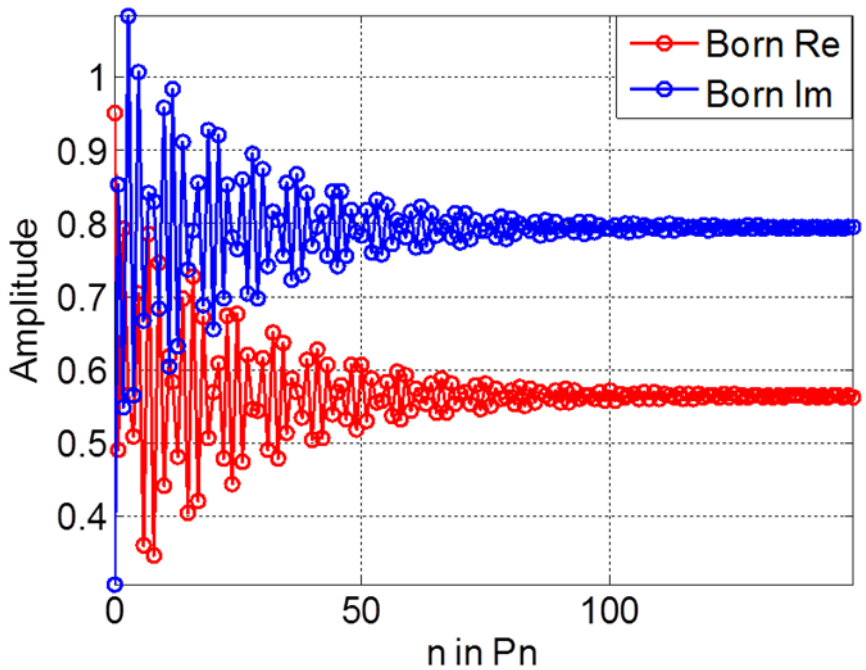

Figure 10. The sequence of complex-valued wavefield of the slowly convergent $\{P_n\}$ at 0.14 Hz. Blue and red lines with circles corresponds to the real and imaginary parts of $\{P_n\}$, respectively.

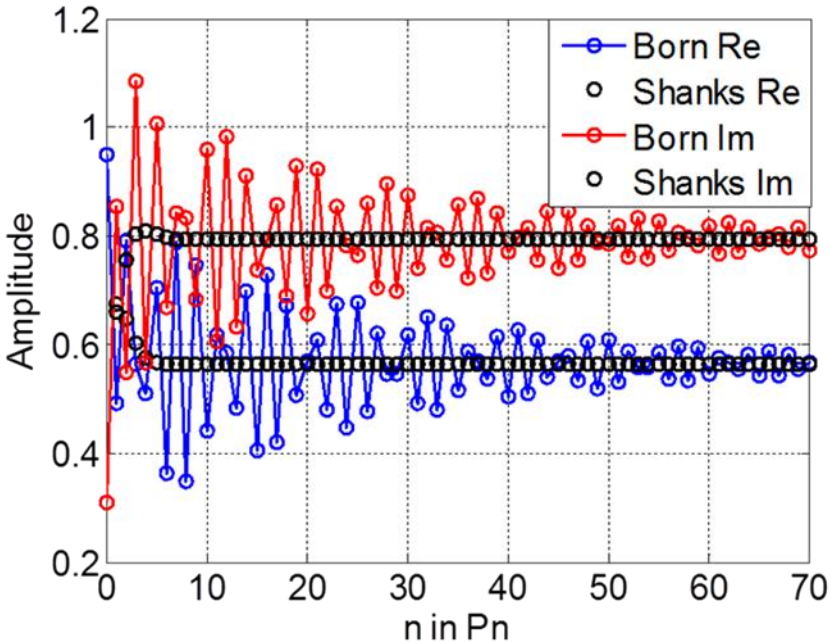

Figure 11. Comparison of the complex-valued Born wavefield P_n and its 3rd order ST at 0.14 Hz for the model in Figure 9. Blue and red lines with circles correspond to the real and imaginary parts of P_n , respectively. Black circle corresponds to the real and imaginary parts of $\{S_n^3[P_n]\}$, respectively.

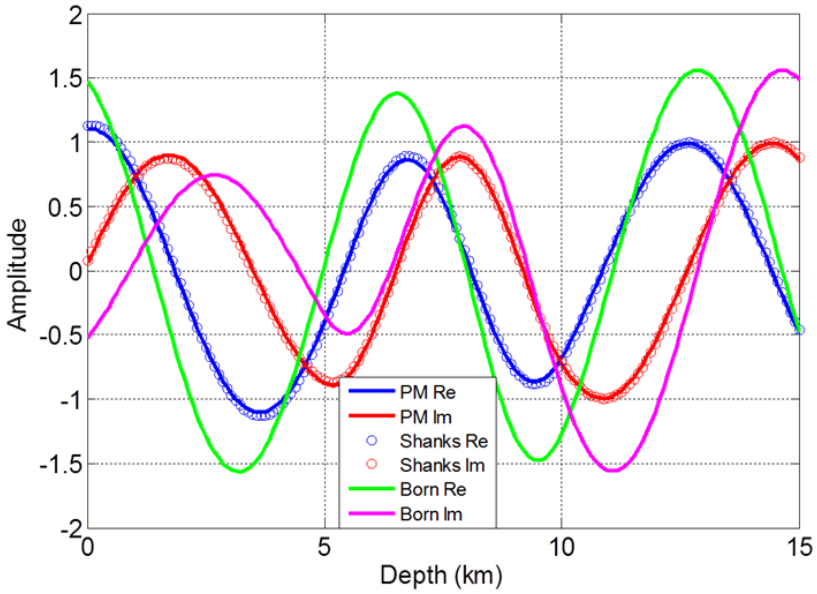

Figure 12. Comparison of the theoretical wavefield calculated by PM method, the *8-th* term of the 3rd ST of the Born wavefield and *8-th* term of Born wavefield without ST. Blue and red solid lines correspond to the real and imaginary parts of theoretical wavefield, respectively. Blue and red circles correspond to the real and imaginary parts of the *8-th* term of the 3rd order ST of the Born wavefield. Green and purple lines correspond to the real and imaginary parts of the *8-th* term of the Born wavefield without ST.

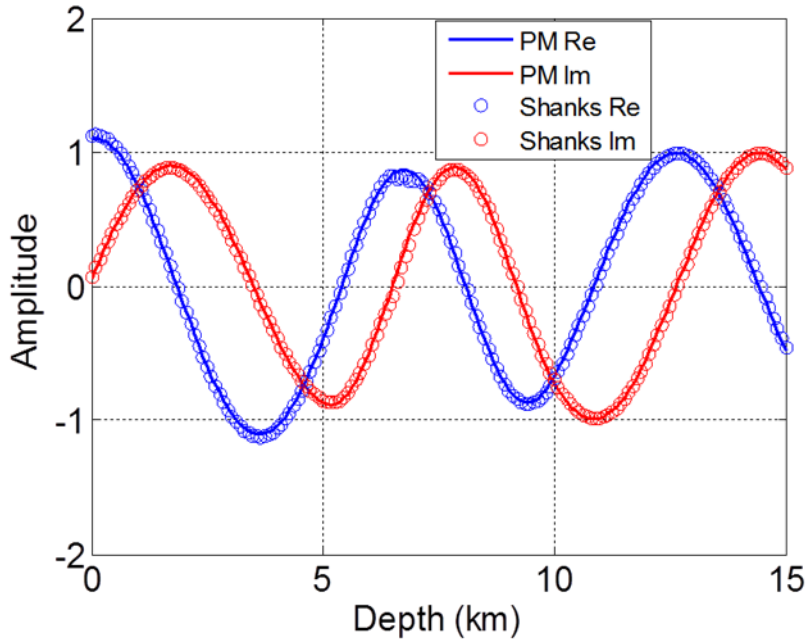

Figure 13. Comparison of the theoretical wavefield calculated by PM method and the *20-th* term of the 3rd order ST of the Born wavefield. Blue and red solid lines correspond to the real and imaginary parts of theoretical wavefield, respectively. Blue and red circles correspond to the real and imaginary parts of the *20-th* term of 3rd order ST of the Born wavefield.

3.7 Application of ST on a divergent Born series

In the third forward modeling example, we use a different model. However, the anomaly-size-to-wavelength ratio is 1.2 with frequency at 25 Hz and reference velocity at 2500 m/s. In this model, we set one high velocity (4000 m/s) layer with thickness of 120 m in a reference medium with velocity of 2500 m/s (Figure 14). This velocity contrast is similar to the case for a salt body in the sedimentary rock. In this case, the Born waveform P_n is divergent for n >10 (Figure 15). Compared with the synthetic wavefield using PM, the Born wavefield diverges around the *10-th* term both in the real and imaginary parts (Figure 16). The divergent Born series gradually converges to the theoretical solution in *5-th* order of ST (Figure 17). On the other hand, the *20-th* term of the *5-th* order ST of the Born wavefield converges to the theoretical wavefield both in the real and imaginary parts (Figure 18). In this example, we can see that the ST can improve the convergence property of series, even for a divergent series.

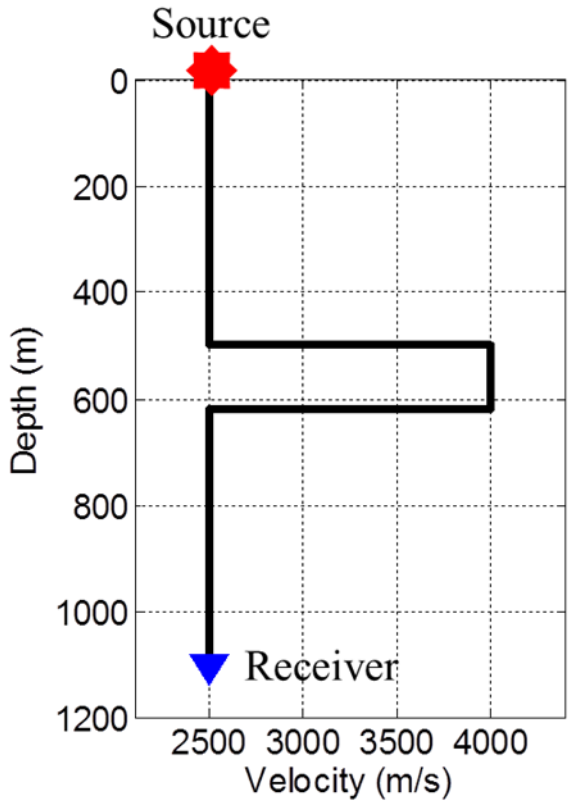

Figure 14. Three-layered model with source (star) and receiver (triangle) located at depth 0 m and 1100 m, respectively. The thickness of anomaly of this model is 120 m.

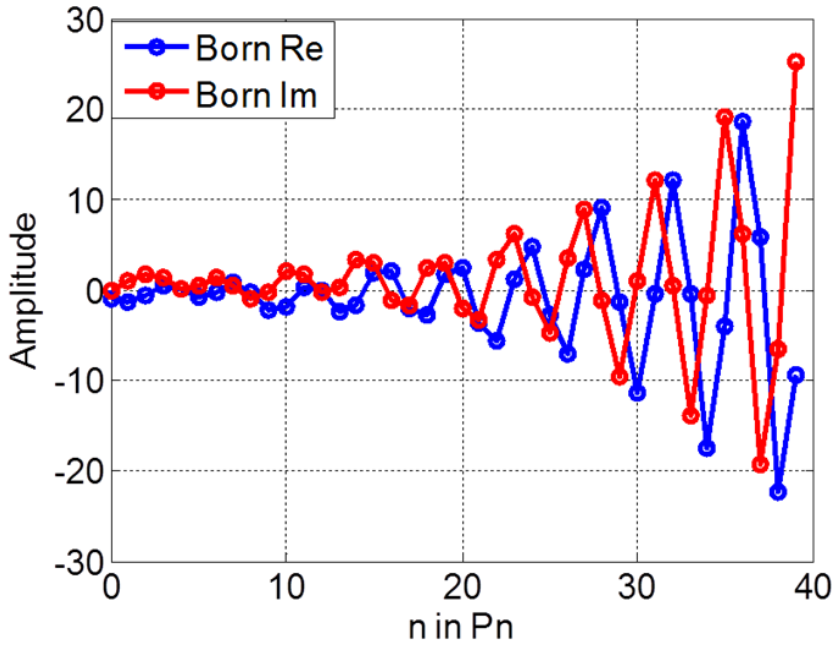

Figure 15. Complex valued of divergent wavefield of P_n .Blue and red lines with circles correspond to the real and imaginary parts of P_n respectively.

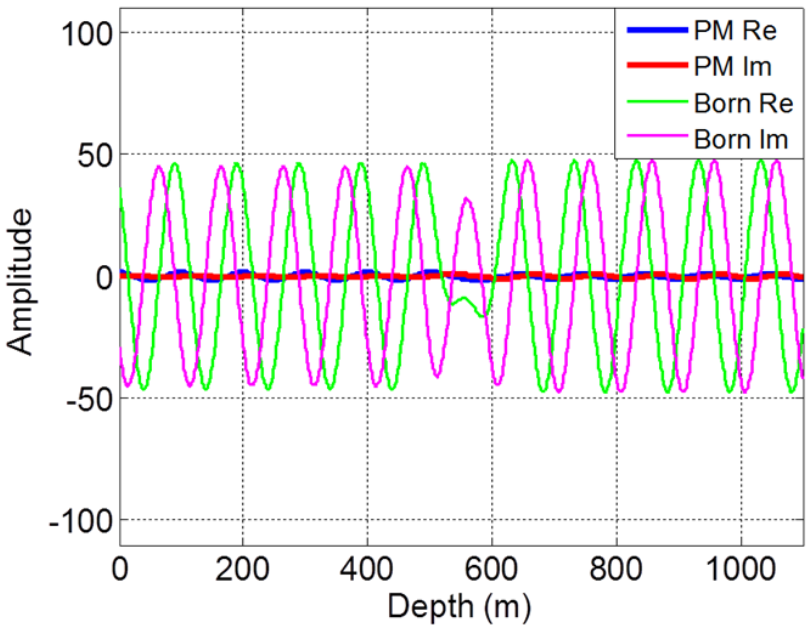

Figure 16. Comparison of the theoretical depth wavefield using PM and the divergent Born wavefield at the *10-th* term. Blue and red lines show the real and imaginary parts of the theoretical wavefield, respectively. Green and purple lines correspond to the real and imaginary parts of the divergent Born wavefield, respectively.

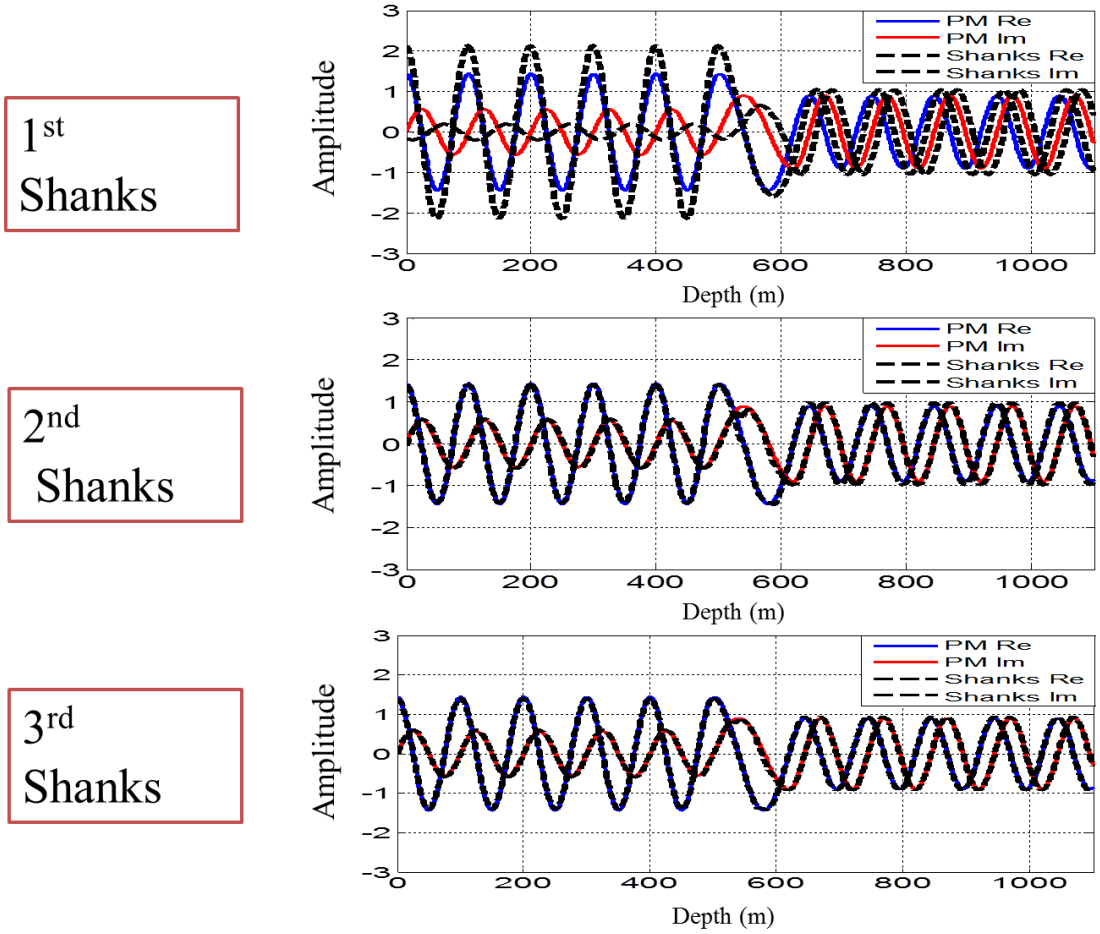

Figure 17. Comparison of the PM wavefield and the *20-th* term of the *1st*, *2nd* and *3rd* orders ST of the Born series.

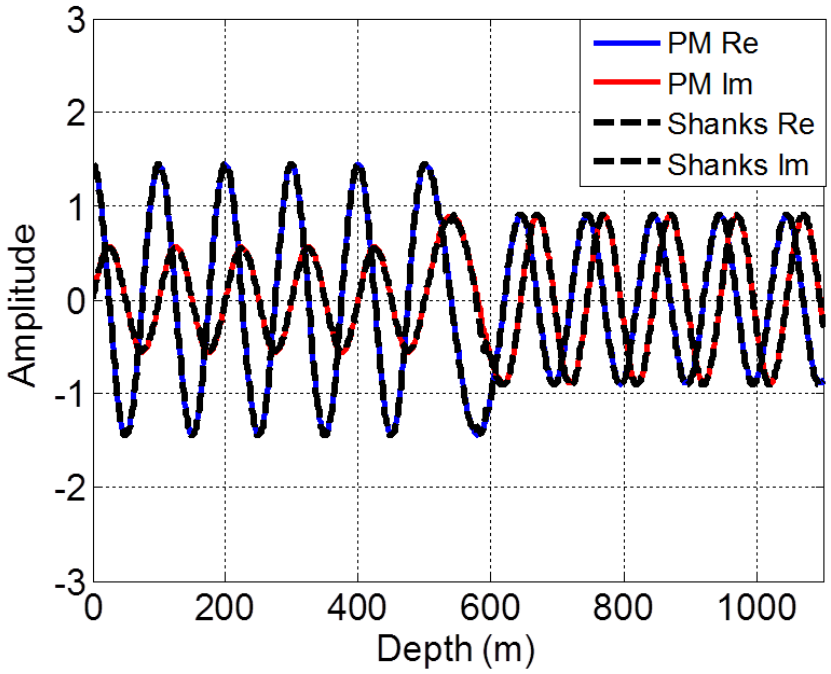

Figure 18. Comparison of the theoretical wavefield using PM and the *20-th* term of the *5-th* order ST of the Born wavefield.

3.8 Summary

In this chapter, using forward Born scattering series, we found ST could be very useful to speed up the convergence for convergent, slowly convergent, and event divergent series. We can always check if the convergent field is the true field by substituting the field into the wave equation.

Chapter 4

Inverse scattering and Shanks Transformation

4.1 Background of seismic exploration

The primary goal of seismic exploration is to produce an accurate map of reflectors below the Earth's surface. This structural map is important to the oil and gas industry because it plays a key role in determining where to drill for hydrocarbon reserves. Weglein et al. (2003) have proposed using the inverse scattering series, a multidimensional direct inversion procedure, to derive a velocity-independent imaging algorithm.

In seismic exploration, a man-made energy source (such as explosion, air gun, hammer, or vibrators) sends an incident wave into the Earth. Rapid changes in Earth properties will cause the incident wave to reflect or diffract and some energy of the reflected wave will return to the surface where it will be recorded by groups of receivers. (A seismic receiver is a device that detects ground motion or a pressure wave in fluid). The reflected wave contains information about the source that created it, the medium that the wave has traveled through, and the inhomogeneity (or

reflectors) that caused part of the incident wave to return to the surface. The recorded seismic data are processed to reveal information about the Earth's subsurface. To produce a seismic image is to generate a subsurface model that can produce the data recorded on the measurement surface. Seismic data in general is a function of source and receiver position and time (t). In order to know where an unknown reflector is located in the Earth, we need to do time-to-depth conversion.

Inverse scattering is a powerful way to image the Earth's subsurface. The solution to the inverse problem is an infinite series, which is called the inverse scattering series (ISS). The reference medium (usually not the true medium), and the source and receiver locations are known in the inverse scattering problems. The subsurface velocities (i.e., the model; we ignore density and other elastic constants for simplicity) are usually different from the reference medium. The difference in seismic velocity between the reference medium and the actual medium is called model perturbation, which is unknown. Finding the velocity perturbation through solving scattering series, we can find the subsurface velocity based on the known reference model.

The recorded data contains many kinds of distinct arrivals of seismic energy, each having a different propagation history from the source to the receiver. Such a distinct arrival of the seismic energy is called a seismic event. It is useful to catalog

and separate these events based on the type and complexity of the interactions they have experienced. Basically, seismic reflection events are catalogued as primary or multiple depending on whether the energy arriving at the receiver has experienced one or more upward reflections, respectively (Figure 19). Multiples can be further classified as free-surface multiples and internal multiples according to whether or not they have been reflected by the free surface or not.

Traditional seismic imaging algorithms assume all acquired seismic events are primary reflections. Multiple data is mapped to wrong location to cause imaging artifacts. Therefore, most imaging methods require the removal of multiples before imaging. The multiple removal is a challenging task. Hence, the new algorithm discussed in this chapter is attractive in application because it does not require multiple removal. Figure 19 represents seismic waves that are studied by scientist to interpret the composition, fluid content, extent and geometry of rocks in the subsurface.

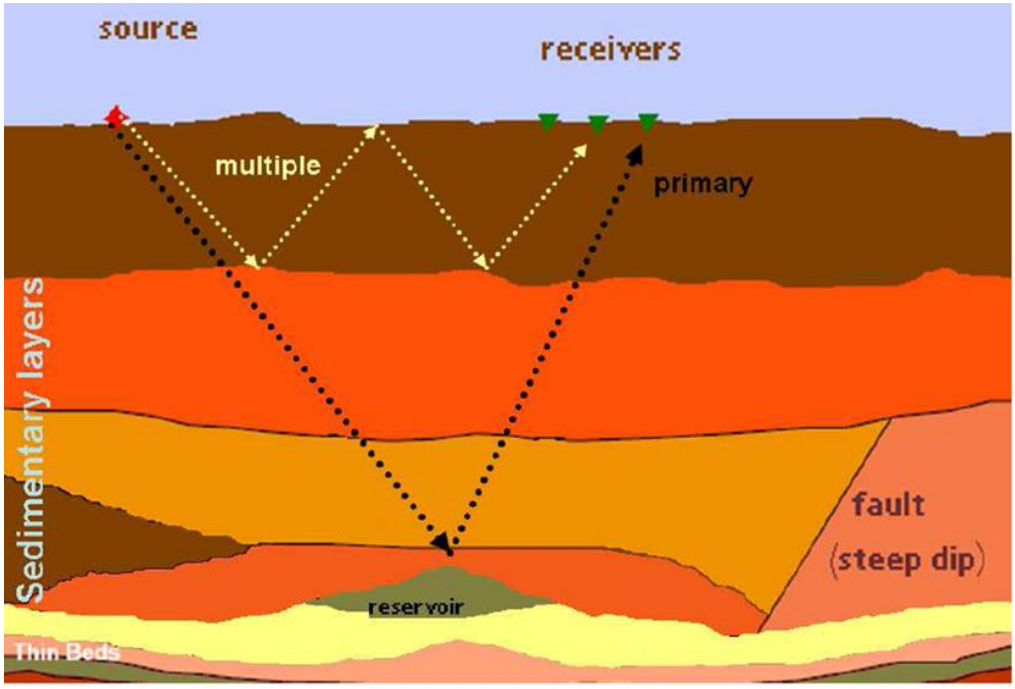

Figure 19. Example of marine case: source (star) and receivers (triangles) are located within the water column. Energy arrivals produced by a single reflection are called primaries. Energy arrivals produced by multiple reverberations are called multiples (From Ramirez (2007)).

4.2 Inverse scattering series introduction

The inverse scattering theory takes the recorded data, $G\left(z_g, z_s, \omega\right)$, to invert for the scattering potential (perturbation) $V\left(z\right)$. Here we follow the formulation of Schlottmann (2006). We start from the Lippmann-Schwinger equation (3.6) and iterate the equation back to itself once and get

$$\begin{aligned} G\left(z_g, z_s, \omega\right) = G_0\left(z_g, z_s, \omega\right) + k_0^2 \int dz' G_0\left(z_g, z', \omega\right) V\left(z'\right) G_0\left(z', z_s, \omega\right) \cdots \\ + \int dz'' G_0\left(z_g, z'', \omega\right) k_0^2 V\left(z''\right) \int dz' G_0\left(z'', z', \omega\right) k_0^2 V\left(z'\right) G\left(z', z_s, \omega\right) \end{aligned}, \quad (4.1)$$

where the left hand side of equation (4.1) is the recorded data. In this dissertation, we let $z_g = z_s = 0$ and $z' > 0$. In the symbolic form, we can have

$$\mathbf{G_{RS}} = \left[\mathbf{G_0}\right]_{RS} + \left[\mathbf{G_0 V G_0}\right]_{RS} + \left[\mathbf{G_0 V G_0 V G}\right]_{RS}, \quad (4.2)$$

where the subscript 'RS' stands for 'recording surface' and it refers to a particular source-receiver geometry; $\mathbf{V}$ is the operator symbol corresponding to the scattering potential $V\left(z\right)$ at each depth; $\mathbf{G}$ is the operator symbol for the 1D Green's function *G*. Note that the 1D Green's function takes a simple form

$$G_0\left(z, z', \omega\right) = \frac{e^{+ik_0\left|z - z'\right|}}{2ik_0}. \quad (4.3)$$

In equation (4.2), the entire wavefield ($\mathbf{G_{RS}}$) can be separated into three terms: background wavefield ($\mathbf{G_0}$), singly-scattered wavefield ($\mathbf{G_0VG_0}$) and multiply-scattered wavefield ($\mathbf{G_0VG_0VG}$). The goal of ISS is to find $\mathbf{V}$ that solves equation (4.2). Let us solve this in an iterative fashion from a starting perturbation model $\mathbf{V}_0$. We hope to obtain a sequence of perturbation models $\mathbf{V}_n$ such that they converge to the true perturbation model $\mathbf{V}$ that can satisfy equation (4.2) or equation (4.1) as

$$\mathbf{V}_0 \rightarrow \mathbf{V}_1 \rightarrow \mathbf{V}_2 \rightarrow \cdots \rightarrow \mathbf{V}_n \cdots \rightarrow \mathbf{V}. \tag{4.4}$$

To accomplish this, let us inspect equation (4.2) in the frequency domain. If we take the inverse Fourier transform of equation (4.2) from the frequency ω domain to the time t domain, we can further convert the inverted perturbation from the t domain into depth z domain based on the velocity model:

$$U(z) - V(z) = \frac{-4}{\pi c_0} \int_{-\infty}^{\infty} \left[\mathbf{G_0VG_0VG}\right]_{RS} e^{-2ikz} d\omega, \tag{4.5}$$

where

$$U(z) = \frac{-4}{\pi c_0} \int_{-\infty}^{\infty} \left[\mathbf{G - G_0}\right]_{RS} e^{-2ikz} d\omega \tag{4.6}$$

is the migration operation using the recorded scattered field and

$$V(z) = \frac{-4}{\pi c_0} \int_{-\infty}^{\infty} \left[\mathbf{G_0 V G}_0 \right]_{RS} e^{-2ikz} d\omega \tag{4.7}$$

is the migration operation acting on a singly scattered wavefield.

Equation (4.5) actually provides a way to update the scattering potential using the residual (multiply-scattered) wavefield:

$$U(z) - V_{n+1}(z) = \frac{-4}{\pi c_0} \int_{-\infty}^{\infty} \left[\mathbf{G_0 V_n G_0 V_n G}^{(n)} \right]_{RS} e^{-2ikz} d\omega, \tag{4.8}$$

where $\mathbf{G}^{(n)}$ is the exact Green's function in the model $V_n(z)$.

In equation (4.8), to obtain the updated scattering potential $V_{n+1}(z)$, the unknown term is the multiply-scattered wavefield. However, directly solution of multiply-scattered wavefield is time consuming. Let us inspect the Lippmann-Schwinger equation (3.8) (after one iteration) again, we find

$$\mathbf{G}^{(n)} = \mathbf{G_0} + \mathbf{G_0 V_n G_0} + \mathbf{G_0 V_n G_0 V_n G}^{(n)}, \tag{4.9}$$

which is an exact (no approximation) equation of the velocity model $\mathbf{V}_n$ (vector symbol of $V_n(z)$). Consequently, we can plug equation (4.9) into equation (4.8) and get

$$V_{n+1}(z) = U(z) - U_n(z) + V_n(z), \tag{4.10}$$

where

$$U_n(z) = \frac{-4}{\pi c_0} \int_{-\infty}^{\infty} \left[\mathbf{G}^{(n)} - \mathbf{G}_0 \right]_{RS} e^{-2ikz} d\omega \tag{4.11}$$

is the migration operation using the calculated scattered field in model $\mathbf{V}_n$ and

$$V_n(z) = \frac{-4}{\pi c_0} \int_{-\infty}^{\infty} \left[\mathbf{G_0} \mathbf{V_n} \mathbf{G_0} \right]_{RS} e^{-2ikz} d\omega . \tag{4.12}$$

Equation (4.10) is the iterative ISS inversion scheme. We can initialize the iterative sequence as

$$V_1(z) = U(z). \tag{4.13}$$

Based on $V_1(z)$, we can compute $U_1(z)$ using equation (4.11) and we can obtain $V_2(z)$ from equation (4.10). This iteration can generate $V_n(z)$ (Appendix C).

Once we obtain the perturbation $V_n(z)$, we can recover the velocity $c_n(z)$ based on the reference velocity (known) $c_0(z)$ in equation (3.7). When the sequence of $c_n(z)$ is available, we can apply the ST:

$$S_n^1[c_n] = \frac{c_{n+1}c_{n-1} - (c_n)^2}{c_{n+1} + c_{n-1} - 2n}, \tag{4.14}$$

where $S_n^1[c_n]$ is the *n-th* term of the first order ST of $\{c_n(z)\}$. We can also construct higher order ST by applying ST more times on the inverted velocity sequence $\{c_n(z)\}$.

4.3 Numerical example

4.3.1 Three-layered velocity model

In the first velocity inversion example, we use a three-layered model (Figure 20) containing a high velocity layer (1.4 km/s) in a reference velocity (1 km/s). The velocity contrast is 40% with respect to the reference velocity. We modeled the waveform observed at the surface receiver using the PM method using the true model, shown in Figure 21. This modeled data is taken as the observed data. In the observed waveform, we can see not only the primary reflections but also the internal multiples. This observed waveform and the reference velocity (1 km/s) are the inputs to the velocity inversion based on the ISS. In the velocity inversion, we use a Gaussian wavelet with a nominal width of 1 s. We can iteratively solve the velocity based on the ISS discussed in the previous section. Several inverted velocity models are shown in Figure 22 and Figure 23, including results at the *1st*, *2nd*, *10-th and 30-th* iterations (without ST). For this three–layered model, the ISS needs 30 iterations to generate a good inverted velocity model (Figure 23). After we obtain a sequence of the inverted

velocity model sequence ($\{c_n\}$), we can apply the ST on $\{c_n\}$. We show the inverted velocity model at *10-th* term of the first order ST of $\{c_n\}$ (Figure 24) and the synthetic waveform produced based on this model Figure 25. We can see that the inverted velocity with the first order ST after 10 iterations can provide a good recovered velocity model. In Figure 26, we show the convergence rate of waveform residuals for velocity inversion without ST and with ST. We can see that the velocity inversion without ST converges at about *30-th* iteration while with the first order ST at *10-th* iteration.

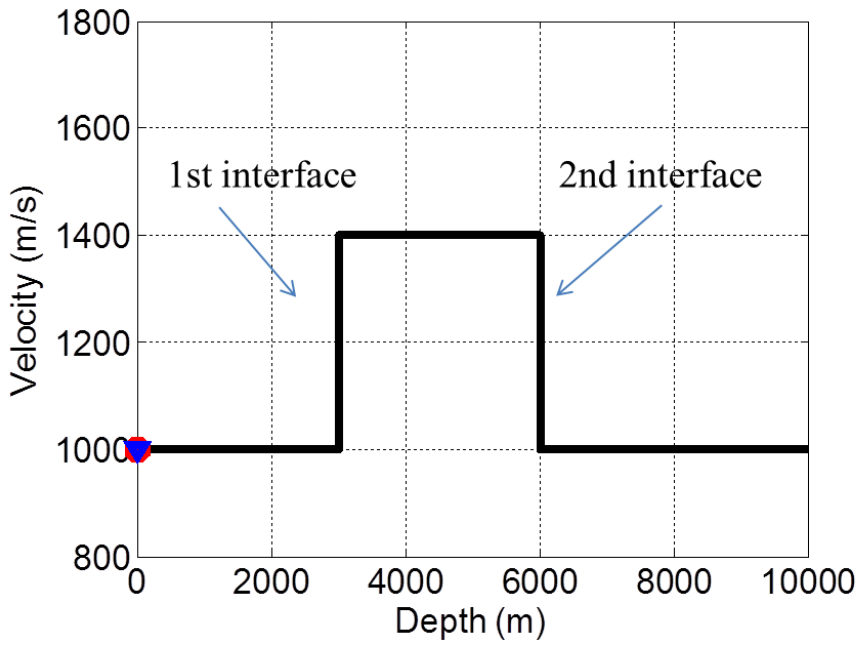

Figure 20: A three-layered velocity model (two interfaces) with both the source (red star) and receiver (blue triangle) deployed on the surface with depth at 0 m. The high-velocity layer (1.4 km/s) has 40% of higher velocity than the reference velocity (1 km/s).

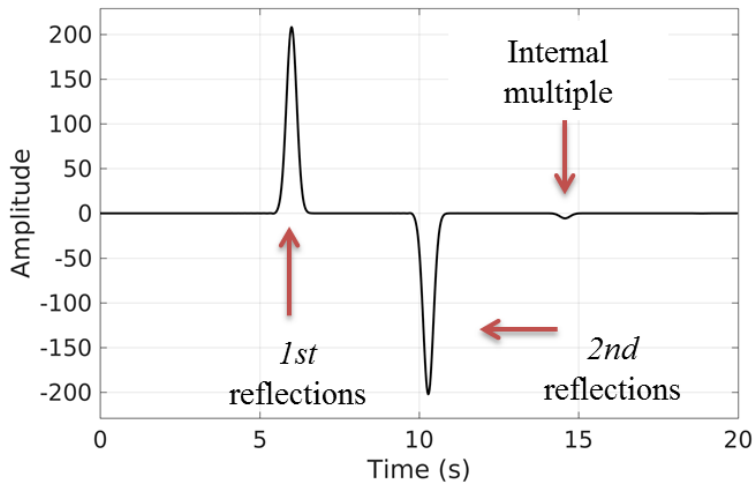

Figure 21. The observed waveform by the receiver at surface (depth at 0 m). The source wavelet is a Gaussian wavelet with a width of 1 s. There are two reflections from the *1st* and *2nd* interfaces and one internal multiples bounced between those two interfaces.

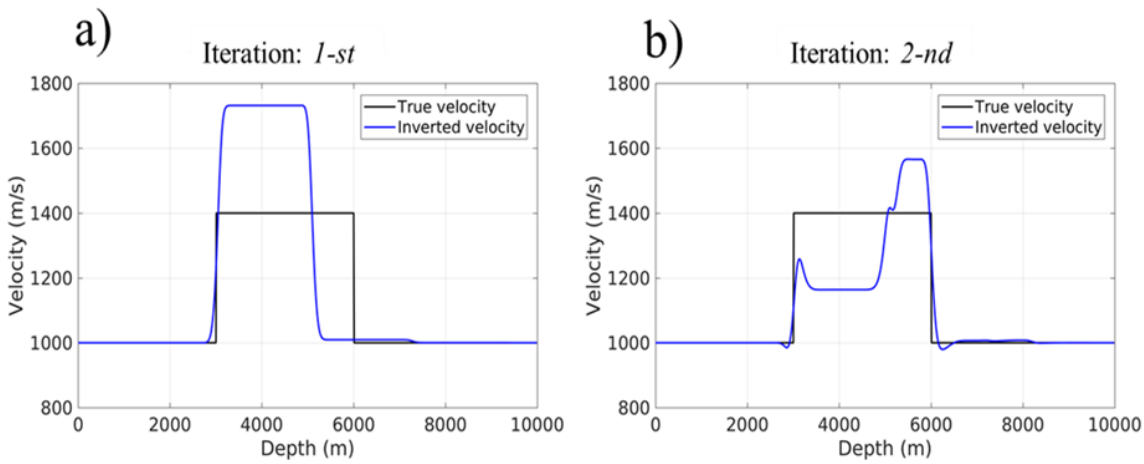

Figure 22. Inverted velocity models based on the ISS (c_n) for the three-layered model (Figure 20) at the (a) *1st*, (b) *2nd*, iteration (without ST), respectively.

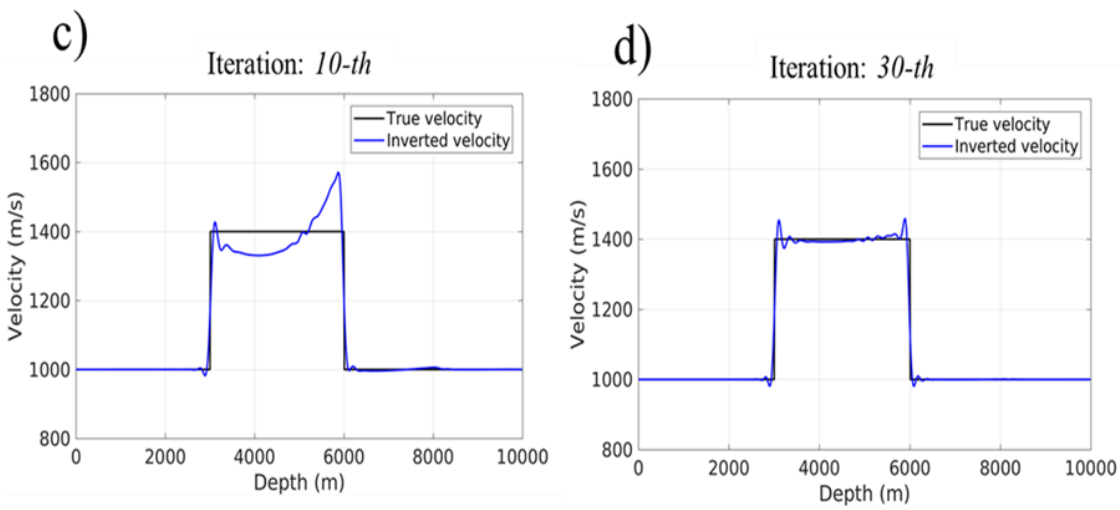

Figure 23. Inverted velocity models based on the ISS (c_n) for the three-layered model (Figure 20) at the (c) *10-th*, (d) *30-th*, iteration (without ST), respectively.

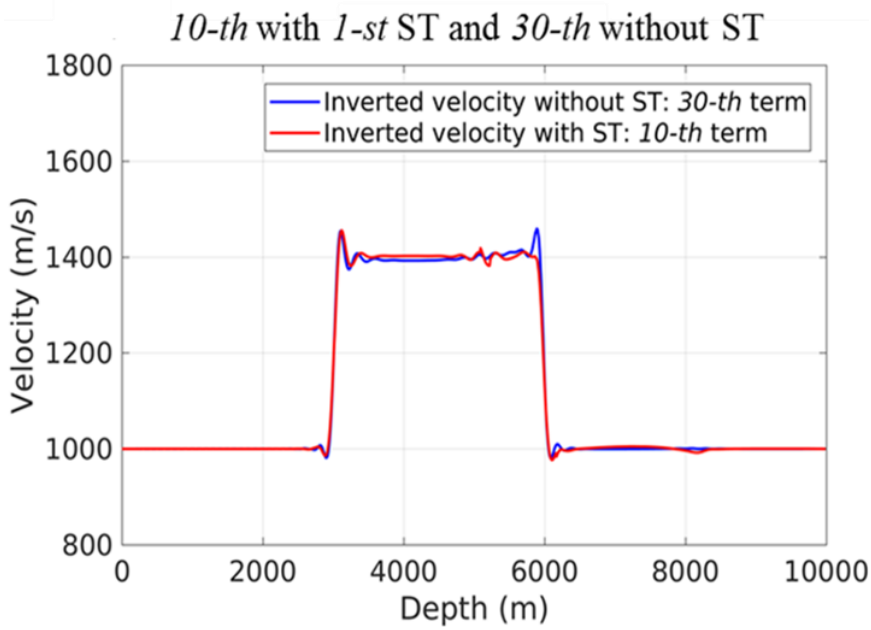

Figure 24. Comparison of the inverted velocity model using ISS with *1st* order of ST at *10-th* iteration (red line) and inverted velocity model without ST at *30-th* iteration (blue line).

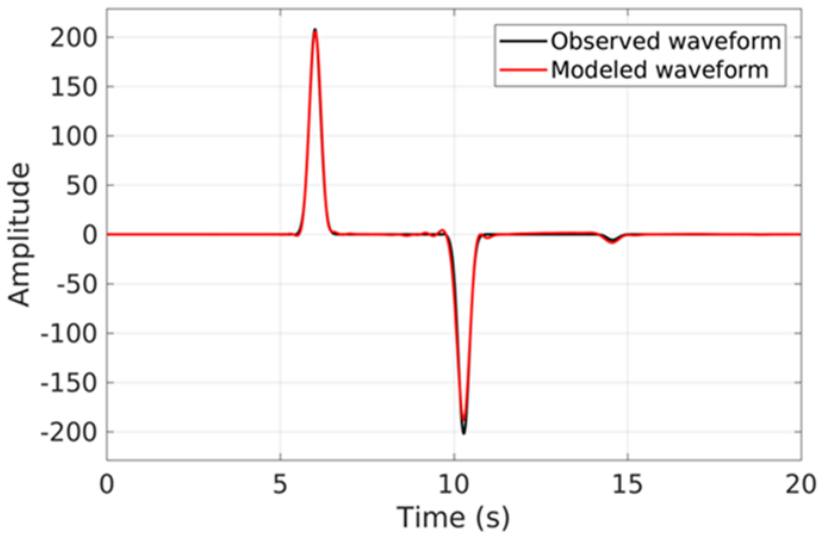

Figure 25. Comparison of the observed waveform (black line) and the modeled waveform using the inverted velocity with the *1st* order ST at *10-th* term. The modeled waveform matches the observed waveform well.

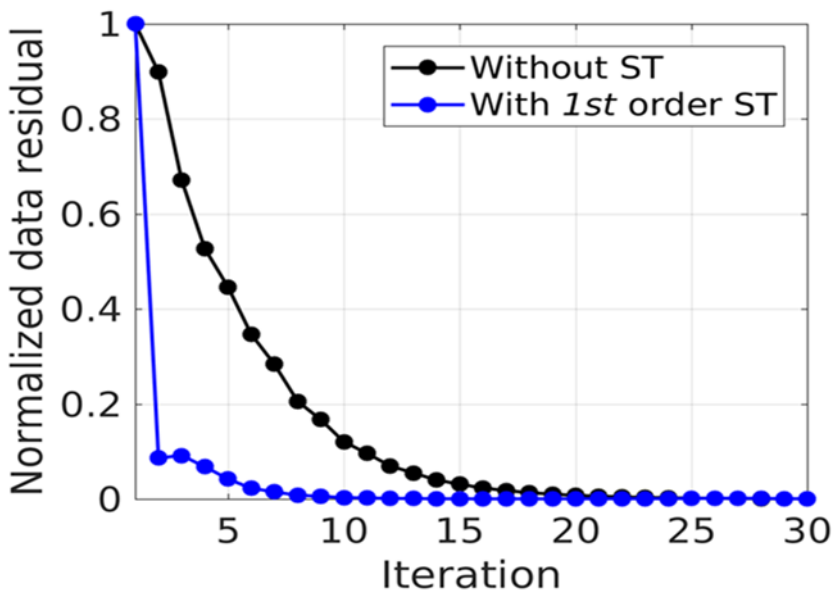

Figure 26. The convergences of the waveform residual between the observed and the modeled waveform. The black line and blue line represent the waveform residual without ST and with the *1*st order ST, respectively.

4.3.2 Seven-layered velocity model

In the second example of velocity inversion, we use a more complex model with seven layers Figure 27. We show the observed waveform using PM method in Figure 28. In the inversion process, we set the initial reference velocity of 1 km/s. Similar to the previous example; we iteratively determine the velocity models based on ISS and then compare the inverted velocity models and their ST. We show some of the inverted velocity models at the *1st*, *2nd*, *7-th*, and *12-th* iteration in Figure 29 and Figure 30. For this seven-layered model, ISS needs 12 iterations to generate a velocity model that close to the true velocity model Figure 30. Then we apply the ST on the sequence of inverted velocity models. We can see that the first order ST can produce a good inverted velocity model after 7 iterations (Figure 31) while the ISS without ST needs 12 iterations to obtain a similar inverted velocity model. From these examples, we can see the ST is effective to accelerate the convergence of iterative velocity inversion based on the ISS for a model with high velocity contrast and multiple layers.

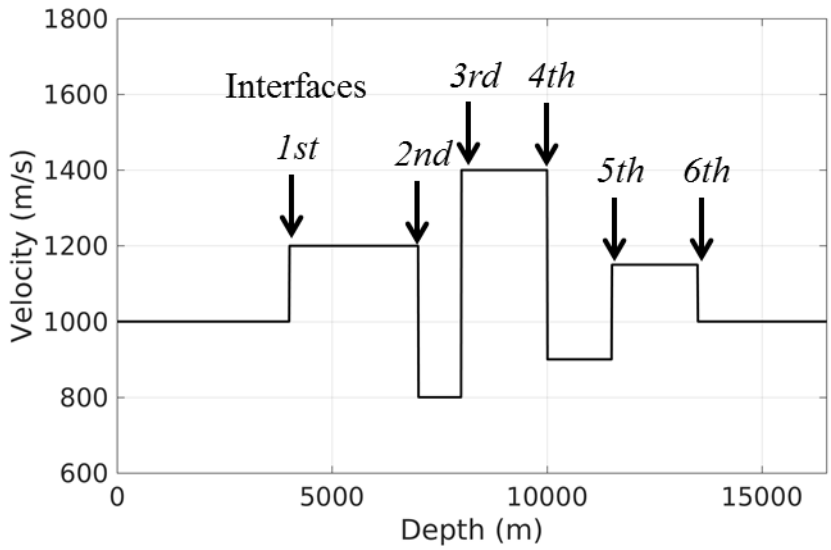

Figure 27. A seven-layered velocity model (6 interfaces) with the source and receiver on the surface at depth 0 m. There are three high-velocity layers and two low-velocity layers with different velocities and thicknesses embedded in the reference medium.

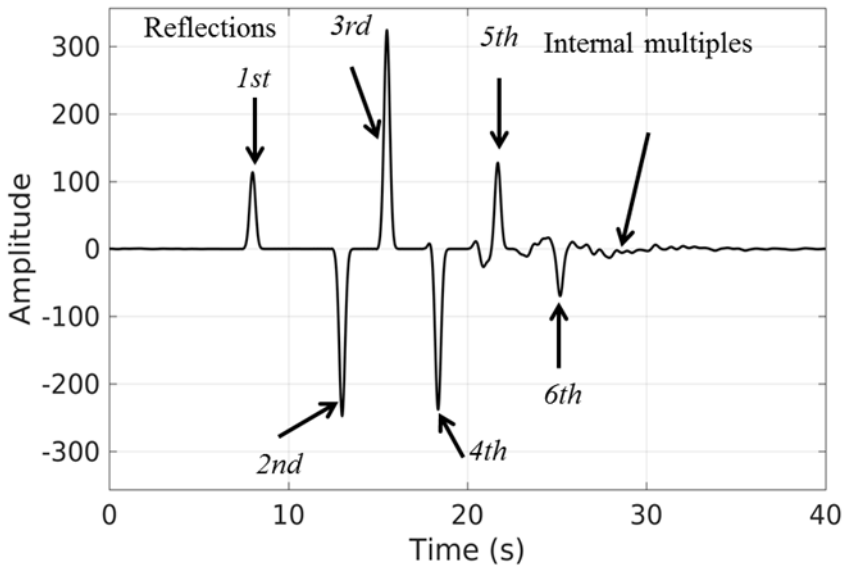

Figure 28. The observed waveform by the receiver at surface. The source wavelet is a Gaussian wavelet with a width of 1 s. There are six reflections from the *1st* to the *6-th* interfaces and several internal multiples bounced between those interfaces.

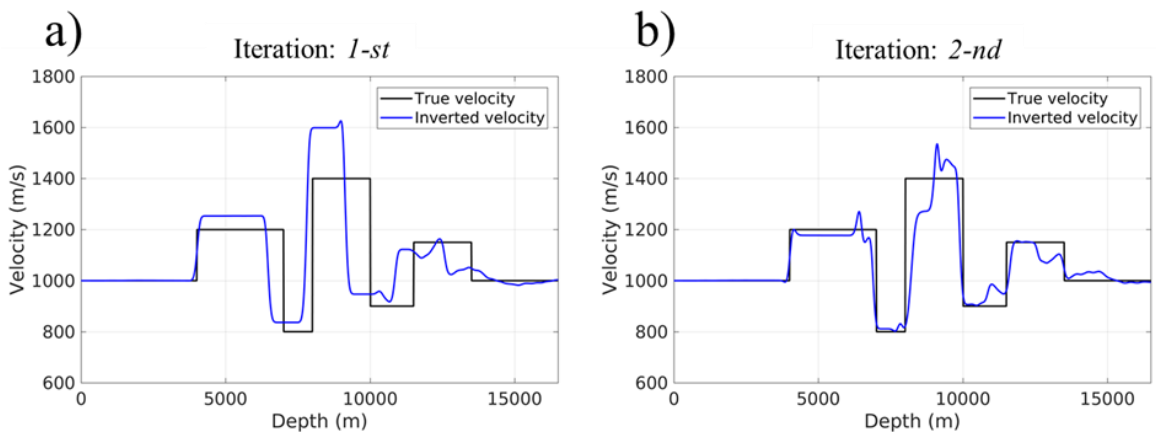

Figure 29. Inverted velocities based on the ISS (c_n) for the seven-layered model (Figure 27) t the (a) *1*st, and (b) *2*nd, iteration, respectively. Blue lines show the inverted velocity model c_n and black lines show the true velocity.

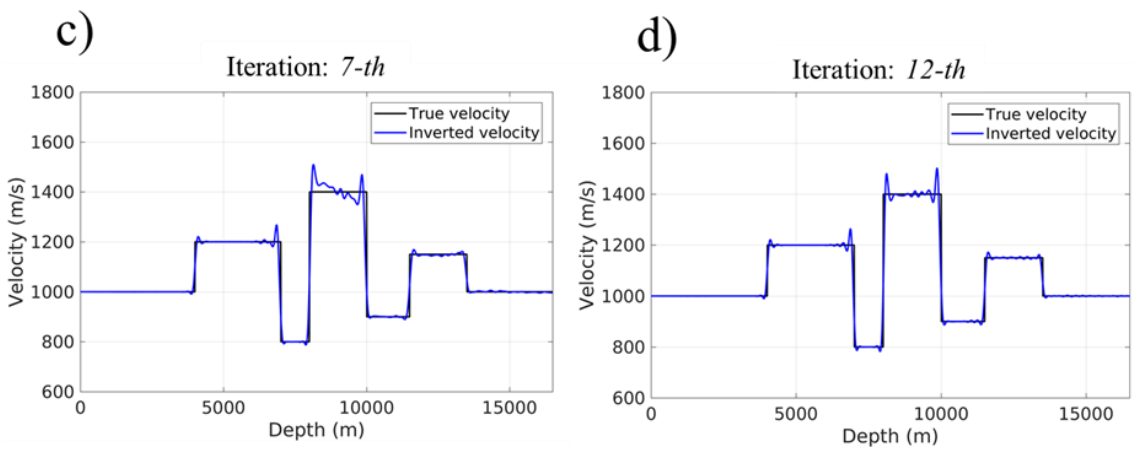

Figure 30. Inverted velocities based on the ISS (c_n) for the seven-layered model (Figure 27) at the (c) *7-th* and (d) *12-th* iteration, respectively. Blue lines show the inverted velocity model c_n and black lines show the true velocity.

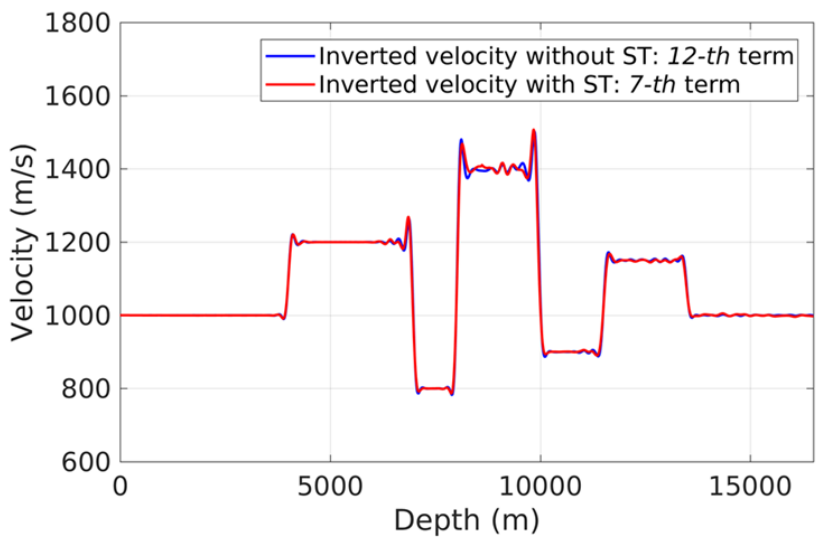

Figure 31. Comparison of the inverted velocity model without ST at the *12-th* iteration (blue line) and the inverted model at *7-th* term of the first order ST (red line).

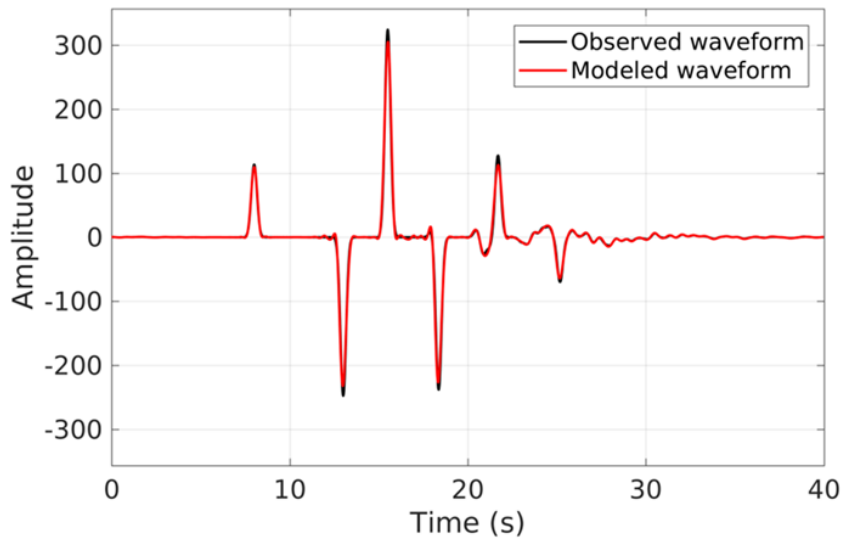

Figure 32. Comparison of the observed waveform (black line) and the modeled waveform using the inverted model (red line) using the inverted velocity at 7-*th* term of the 1st order ST. The modeled waveform well matches the observed waveform for both primary reflections and multiples.

Chapter 5

Conclusions and future work

The scattering series is commonly used for solving the forward and inverse problem in the seismic applications. Shanks Transformation (ST) is an effective method to improve the convergence of the scattering series. ST separates the series into a secular trend and an oscillatory transient term and emphasizes the convergence of the secular term. In this regard, the ST is suitable to sum up the scattering series. ST is a nonlinear local operation, which means we do not need to pre-compute all terms in the scattering series before we can produce an output. We showed that the ST could accelerate the convergence of the forward modeling using the Born series for three examples, including summing up a divergent series to obtain the correct wavefield. In the velocity inversion based on ISS, we showed that ST could again speed up the convergence for a model with large velocity contrasts and multiple layers. Since in seismic inversion problems, the iterative process, such as full-waveform-inversion (FWI), is used frequently, applying the ST may greatly facilitate the computation in both detecting the limit and actually finding the limit fast. Therefore, ST provides a useful tool for inverting large-contrast medium perturbation in seismic inversion problems.

These examples in this dissertation are layered models. In unconventional oil/gas exploration and development, most of the geological structures are simple and layered. Therefore, the approach laid out in this thesis can be immediately used. It is not clear whether Shanks method in complex models can still be as powerful as for layered cases. However, given the success achieve in the thesis, developing of ST application on the real dataset in 2D and 3D models can be addressed as a new challenge for future studies.

REFERENCES

Aki, K., and P. G. Richards. 2002, *Quantitative Seismology*: University Sciences Books.

Alkhalifah, T. 2000, Prestack phase-shift migration of separate offsets. *Geophysics*, **65**, no. 4,1179-1194.

Alkhalifah, T. 2010, Acoustic wavefield evolution as a function of source location perturbation. *Geophysical Journal International*, **183**, no. 3,1324-1331.

Alkhalifah, T. 2013a, Residual extrapolation operators for efficient wavefield construction. *Geophysical Journal International*, **193**, no. 2,1027-1034.

Alkhalifah, T. 2013b, Traveltime approximations for inhomogeneous transversely isotropic media with a horizontal symmetry axis. *Geophysical Prospecting*, **61**, no. 3,495-503.

Bender, C. M., and S. A. Orszag. 1978, *Advanced mathematical methods for scientists and engineers*: McGraw-Hill.

Brezinski, C. 1982, Some New Convergence *Acceleration Methods. Mathematics of Computation*, **39**, no. 159,133-145.

Chou, C. C., J. Yao, and D. J. Kouri. 2017, Volterra inverse scattering series method for one-dimensional quantum barrier scattering. *International Journal of Quantum Chemistry*, **117**, no. 17.

Clayton, R. W., and R. H. Stolt. 1981, A Born-Wkbj Inversion Method for Acoustic Reflection Data. *Geophysics*, **46**, no. 11,1559-1567.

Cohen, J. K., and N. Bleistein. 1977, An inverse method for determining small variations in propagation speed. SIAM *Journal on Applied Mathematics*, **32**, no. 4,784-799.

Erricolo, D. 2003, Acceleration of the Convergence of Series Containing Mathieu Functions Using Shanks Transformation. *Ieee* Antennas and Wireless Propagation Letters, **2**,58-61.

Grotendorst, J., and E. O. Steinborn. 1986, Use of Nonlinear Convergence Accelerators for the Efficient Evaluation of Gto Molecular Integrals. *Journal of Chemical Physics*, **84**, no. 10,5617-5623.

Haskell, N. A. 1953, The dispersion of surface waves on multilayered media. Bulletin of the *Seismological Society of America*, **43**, no. 1,17-34.

Levin, D. 1972, Development of non-linear transformations for improving convergence of sequences. International *Journal of Computer Mathematics*, **3**, no. 1-4,371-388. doi: 10.1080/00207167308803075.

Liang, H. 2013, Addressing several key outstanding issues and extending the capability of the inverse scattering subseries for internal multiples attenuation, depth imaging, and parameter estimation. *PhD. dissiertation*, University of Houston.

Luo, Y., P. G. Kelamis, Q. Fu, S. Huo, G. Sindi, S.-Y. Hsu, and A. B. Weglein. 2011, Elimination of land internal multiples based on the inverse scattering series. *The Leading Edge*, **30**, no. 8,884-889.

Matson, K. 1996, The relationship between scattering theory and the primaries and multiples of reflection seismic data. *Journal of Seismic Exploration*, **5**, no. 1,63-78.

Newton, R. G. 2013, Scattering theory of waves and particles: *Springer Science* & *Business Media.*

Ramirez, A. C. 2007, Inverse scattering subseries for removal of internal multiples and depth imaging primiaries. *Ph.D. dissertation,* Univesity of Houston.

Sams, W. N., and D. J. Kouri. 1969, Noniterative Solutions of Integral Equations for Scattering .I. Single Channels. *Journal of Chemical Physics*, **51**, no. 11,4809-&.

Schlottmann, R. B. 2006, Direct waveform inversion via iterative inverse propagation, SEG Technical Program Expanded Abstracts 2006: Society of Exploration *Geophysicists.* 2146-2150.

Shanks, D. 1955, Non-linear Transformations of Divergent and Slowly Convergent Sequences. Studies in *Applied Mathematics*, **34**, no. 1-4,1-42.

Shaw, S. A, 2005, An inverse scattering series algorithm for depth imaging of reflection data from a layered acoustic medium with an unknown velocity model. *PhD. dissertation*, University of Houston.

Singh, S., W. F. Richards, J. R. Zinecker, and D. R. Wilton. 1990, Accelerating the Convergence of Series Representing the Free Space Periodic Green-Function. *Ieee* Transactions on Antennas and Propagation, **38**, no. 12,1958-1962.

Singh, S., and R. Singh. 1991, On the Use of Shanks Transform to Accelerate the Summation of Slowly Converging Series. *Ieee* Transactions on Microwave Theory and Techniques, **39**, no. 3,608-610.

Smith, D. A., and W. F. Ford. 1979, Acceleration of Linear and Logarithmic Convergence. Siam *Journal on Numerical Analysis*, **16**, no. 2,223-240.

Stolt, R. H., and A. B. Weglein. 1985, Migration and Inversion of Seismic Data. *Geophysics*, **50**, no. 12,2458-2472.

Stovas, A., and T. Alkhalifah. 2012, A new traveltime approximation for TI media. *Geophysics*, **77**, no. 4,C37-C42.

Tarantola, A. 1984, Inversion of Seismic-Reflection Data in the Acoustic Approximation. *Geophysics*, **49**, no. 8,1259-1266. doi: Doi 10.1190/1.1441754.

Tarantola, A. 2005, *Inverse problem* theory and methods for model parameter estimation: SIAM.

Taylor, J. R. 2012, Scattering theory: *the quantum theory of nonrelativistic* collisions: Courier Corporation.

Wang, M., and B. Hung. 2014, 3D Inverse Scattering Series Method for Internal Multiple Attenuation. Paper read at 76th *EAGE Conference* and Exhibition 2014.

Weglein, A., F. Gasparotto, P. Carvalho, and R. Stolt. 1997, An inverse-scattering series method for attenuating multiples in seismic reflection data. *Geophysics*, **62**, no. 6,1975-1989. doi: 10.1190/1.1444298.

Weglein, A., Fang Liu, Xu Li, Paolo Terenghi, Ed Kragh, James D. Mayhan, Zhiqiang Wang, Joachim Mispel, Lasse Amundsen, Hong Liang, Lin Tang, and S.-Y. Hsu. 2012, Inverse scattering series direct depth imaging without the velocity model: First field data examples. *Journal of Seismic Exploration*, **21**,1-28.

Weglein, A. B. 2013, A timely and necessary antidote to indirect methods and so-called P-wave FWI. *The Leading Edge*, **32**, no. 10,1192-1204.

Weglein, A. B. 2017, A direct inverse method for subsurface properties: The conceptual and practical benefit and added value in comparison with all current indirect methods, for example, amplitude-variation-with-offset and full-waveform inversion. *Interpretation*, **5**, no. 3,SL89-SL107.

Weglein, A. B., F. V. Araujo, P. M. Carvalho, R. H. Stolt, K. H. Matson, R. T. Coates, D. Corrigan, D. J. Foster, S. A. Shaw, and H. Y. Zhang. 2003, Inverse scattering series and seismic exploration. *Inverse Problems*, **19**, no. 6,R27-R83.

Weglein, A. B., H. Y. Zhang, A. C. Ramirez, F. Liu, and J. E. M. Lira. 2009, Clarifying the underlying and fundamental meaning of the approximate linear inversion of seismic data. *Geophysics*, **74**, no. 6,Wcd1-Wcd13.

Weniger, E. J. 1989, Nonlinear Sequence Transformations for the Acceleration of Convergence and the Summation of Divergent Series. *Computer Physics Reports*, **10**, no. 5-6,191-371.

Weniger, E. J., J. Grotendorst, and E. O. Steinborn. 1985, Some Applications of Nonlinear Convergence Accelerators. *International Journal of Quantum Chemistry*,181-191.

Wu, R.-S. 1994, Wide-angle elastic wave one-way propagation in heterogeneous media and an elastic wave complex-screen method. *Journal of Geophysical* Research, **99**, no. B1,751-766.

Wu, R.-S., and K. Aki. 1988, Introduction: Seismic wave scattering in three-dimensionally heterogeneous earth. Pure and *Applied Geophysics*, **128**, no. 1-2,1-6.

Wu, R.-S., and Y. Zheng. 2014, Non-linear partial derivative and its De Wolf approximation for non-linear seismic inversion. *Geophysical Journal International*, **196**, no. 3,1827-1843.

Yao, J., A. C. Lesage, B. G. Bodmann, F. Hussain, and D. J. Kouri. 2014a, Inverse scattering theory: Inverse scattering series method for one dimensional non-compact support potential. *Journal of Mathematical Physics*, **55**, no. 12.

Yao, J., A. C. Lesage, B. G. Bodmann, F. Hussain, and D. J. Kouri. 2014b, One dimensional acoustic direct nonlinear inversion using the Volterra inverse scattering series. *Inverse Problems*, **30**, no. 7.

Yao, J., A. C. Lesage, F. Hussain, and D. J. Kouri. 2016, Forward Scattering and Volterra Renormalization for Acoustic Wavefield Propagation in Vertically Varying Media. Communications in *Computational Physics*, **20**, no. 2,353-373.

Zhang, H. 2006, Direct non-linear acoustic and elastic inversion: towards fund amentally new comprehensive and realistic target identification. *PhD. dissertation*, University of Houston.

Zuberi, M. A. H., and T. Alkhalifah. 2014a, Generalized internal multiple imaging. *Geophysics*, **79**, no. 5,S207-S216.

Zuberi, M. A. H., and T. Alkhalifah. 2014b, Generalized internal multiple imaging (GIMI) using Feynman-like diagrams. *Geophysical Journal International*, **197**, no. 3,1582-1592.

APPENDICES

A.Forward modeling using the Born series

For acoustic waves propagating in an inhomogeneous media of constant density with source located at z_s and receiver located at z_g, the Green's function $G(z_g, \omega; z_s)$ in the frequency ω domain can be represented as (Clayton and Stolt 1981):

$$G(z_g, \omega; z_s) = G_0(z_g, \omega; z_s) + \frac{\omega^2}{c_0^2} \int_{-\infty}^{\infty} dz' G_0(z_g, \omega; z') V(z') G(z', \omega; z_s), \tag{A-1}$$

where $k = \frac{\omega}{c_0}$ is the wavenumber in the background (reference) medium;

$$V(z) = 1 - \frac{{c_0}^2}{c(z)^2} \tag{A-2}$$

is the scattering potential (perturbation) at depth z; $c_0(z)$ and $c(z)$ are the reference velocity and the true velocity in depth z domain, respectively; $G_0(z_g, \omega; z_s)$ is the Green's function in the reference velocity c_0 from the source z_s to the receiver z_g and $G(z_g, \omega; z_s)$ is the Green's function for the true medium $c(z)$. Equation (A-1) is also called as Lippmann-Schwinger equation. Iterating equation (A-1) back to itself generate the Born series

$$G_1\left(z_g,\omega;z_s\right)=G_0\left(z_g,\omega;z_s\right)+\frac{\omega^2}{c_0^2}\int_{-\infty}^{\infty}dz'G_0\left(z_g,\omega;z'\right)V\left(z'\right)G_0\left(z',\omega;z_s\right),$$

$$G_1\left(z_g,\omega;z_s\right)=p_0+p_1\,. \tag{A-3}$$

Equation (A-3) is the first order Born approximation, p_0 and p_1 are the first and second terms of the Born Series .The Green's function with second order Born approximation can be obtained by replacing G in the equation (A-3) into the right hand side of equation (A-1) and get

$$\begin{aligned}G_2\left(z_g,\omega;z_s\right)&=G_0\left(z_g,\omega;z_s\right)\\&+\frac{\omega^2}{c_0^2}\int_{-\infty}^{\infty}dz'G_0\left(z_g,\omega;z'\right)V\left(z'\right)G_0\left(z',\omega;z_s\right)\\&+\frac{\omega^4}{c_0^4}\int_{-\infty}^{\infty}dz'\int_{-\infty}^{\infty}dz''G_0\left(z_g,\omega;z'\right)V\left(z'\right)G_0\left(z',\omega;z''\right)\mathrm{V}\left(z''\right)G_0\left(z'',\omega;z_s\right)\end{aligned}\quad. \tag{A-4}$$

Let P_0, P_1 and P_2 denote the three terms in the above equation, then $G_2\left(z_g,\omega;z_s\right)$ can be written as

$$G_2\left(z_g,\omega;z_s\right)=p_0+p_1+p_2\,. \tag{A-5}$$

We can iteratively calculate the G as

$$G_n\left(z_g,\omega;z_s\right)=G_0\left(z_g,\omega;z_s\right)+\frac{\omega^2}{c_0^2}\int_{-\infty}^{\infty}dz'G_0\left(z_g,\omega;z'\right)V\left(z'\right)G_{n-1}\left(z',\omega;z_s\right),$$

$$G_n\left(z_g, \omega; z_s\right) = p_0 + p_1 + p_2 + \ldots = \sum_{i=0}^{n} p_i \,, \tag{A-6}$$

where G_n indicates the Green's function with *n-th* order Born approximation; p_i is the *i-th* term of Born series.

B. Derivation of reflection and transmission coefficient from PM method

For a simple three-layered model which is shown in chapter three, our goal is to find the pressure wavefield in the actual medium as following.

Pressure wavefield for each layer will be defined as:

$$P_1 = e^{ik_0 z} + Re^{-ik_0 z}, \qquad \text{First layer} \qquad \text{(B-1)}$$

$$P_2 = A_1 e^{ik_1 z} + A_2 e^{-ik_1 z}, \qquad \text{Second layer} \qquad \text{(B-2)}$$

$$P_3 = Te^{ik_0 z}. \qquad \text{Third layer} \qquad \text{(B-3)}$$

The total wavefield $P = P_1 + P_2 + P_3$, and in order to find R, A_1, A_2 and T, all of the above equations and their derivatives should be continuous at the boundaries z_1, z_2. Therefore we have continuity at the first barrier $z = z_1$ as

$$P_1 = P_2 \text{ at } z = z_1, \qquad \text{(B-4)}$$

$$e^{ik_0 z_1} + Re^{-ik_0 z_1} = A_1 e^{ik_1 z_1} + A_2 e^{-ik_1 z_1}, \qquad \text{(B-5)}$$

$$Re^{-ik_0 z_1} - A_1 e^{ik_1 z_1} - A_2 e^{-ik_1 z_1} = -e^{ik_0 z_1}, \qquad \text{(B-6)}$$

where

$$\begin{cases} A(1,1) = e^{-ik_0 z_1} \\ A(1,2) = -e^{ik_1 z_1} \\ A(1,3) = -e^{-ik_1 z_1} \\ A(1,4) = 0 \end{cases} \qquad B(1) = -e^{ik_0 z_1}. \tag{B-7}$$

For the second interface at the barrier $z = z_2$, we have

$$P_2 = P_3 \text{ at } z = z_2, \tag{B-8}$$

$$A_1 e^{ik_1 z_2} + A_2 e^{-ik_1 z_2} = T e^{ik_0 z_2}, \tag{B-9}$$

where

$$\begin{cases} A(2,1) = 0 \\ A(2,2) = e^{ik_1 z_2} \\ A(2,3) = e^{-ik_1 z_2} \\ A(2,4) = -e^{ik_0 z_2} \end{cases} \qquad B(2) = 0. \tag{B-10}$$

The derivative of the equations (B-1) and (B-2) should be continuous at boundaries as well. Therefore

$$\frac{\partial P_1}{\partial z} = \frac{\partial P_2}{\partial z} \text{ at } z = z_1. \tag{B-11}$$

The derivative of equation (B-5) will be

$$ik_0 e^{ik_0 z_1} - ik_0 R e^{-ik_0 z_1} = ik_1 A_1 e^{ik_1 z_1} - ik_1 A_2 e^{-ik_1 z_1}, \tag{B-12}$$

where

$$\begin{cases} A(3,1) = -ik_0 e^{-ik_0 z_1} \\ A(3,2) = -ik_1 e^{ik_1 z_1} \\ A(3,3) = ik_1 e^{-ik_1 z_1} \\ A(3,4) = 0 \end{cases} \qquad B(3) = -ik_0 e^{ik_0 z_1}. \tag{B-13}$$

The derivative of equations (B-2) and (B-3) for second barrier should satisfy equation (B-15)

$$\frac{\partial P_2}{\partial z} = \frac{\partial P_3}{\partial z} \text{ at } z = z_2, \tag{B-14}$$

$$ik_1 e^{ik_1 z_2} A_1 - ik_1 e^{-ik_1 z_2} A_2 - ik_0 e^{ik_0 z_2} T = 0. \tag{B-15}$$

where

$$\begin{cases} A(4,1) = 0 \\ A(4,2) = ik_1 e^{ik_1 z_2} \\ A(4,3) = -ik_1 e^{-ik_1 z_2} \\ A(4,4) = -ik_0 e^{ik_0 z_2} \end{cases} \qquad B(4) = 0. \tag{B-16}$$

Now we have four equations with four unknowns, equations (B-17) to (B-20) are the equations that we need to solve

$$e^{-ik_0 z_1} R - e^{ik_1 z_1} A_1 - e^{-ik_1 z_1} A_2 = -e^{ik_0 z_1}, \tag{B-17}$$

$$e^{ik_1 z_2} A_1 + e^{-ik_1 z_2} A_2 - e^{ik_0 z_2} T = 0, \tag{B-18}$$

$$-ik_0 e^{-ik_0 z_1} R - ik_1 e^{ik_1 z_1} A_1 + ik_1 e^{-ik_1 z_1} A_2 = -ik_0 e^{ik_0 z_1}, \tag{B-19}$$

$$ik_1 e^{ik_1 z_2} A_1 - ik_1 e^{-ik_1 z_2} A_2 - ik_0 e^{ik_0 z_2} T = 0. \tag{B-20}$$

We can rewrite the above equations in Matrix format as

$$\begin{bmatrix} e^{-ik_0 z_1} & -e^{ik_1 z_1} & -e^{-ik_1 z_1} & 0 \\ 0 & e^{ik_1 z_2} & e^{-ik_1 z_2} & -e^{-ik_0 z_2} \\ -ik_0 e^{-ik_0 z_1} & -ik_1 e^{ik_1 z_1} & ik_1 e^{-ik_1 z_1} & 0 \\ 0 & ik_1 e^{ik_1 z_2} & -ik_1 e^{-ik_1 z_2} & -ik_0 e^{ik_0 z_2} \end{bmatrix} \times \begin{bmatrix} R \\ A_1 \\ A_2 \\ T \end{bmatrix} = \begin{bmatrix} -e^{ik_0 z_1} \\ 0 \\ -ik_0 e^{ik_0 z_1} \\ 0 \end{bmatrix}. \tag{B-21}$$

Thus we can solve the coefficients

$$\begin{bmatrix} R \\ A_1 \\ A_2 \\ T \end{bmatrix} = \begin{bmatrix} e^{-ik_0 z_1} & -e^{ik_1 z_1} & -e^{-ik_1 z_1} & 0 \\ 0 & e^{ik_1 z_2} & e^{-ik_1 z_2} & -e^{-ik_0 z_2} \\ -ik_0 e^{-ik_0 z_1} & -ik_1 e^{ik_1 z_1} & ik_1 e^{-ik_1 z_1} & 0 \\ 0 & ik_1 e^{ik_1 z_2} & -ik_1 e^{-ik_1 z_2} & -ik_0 e^{ik_0 z_2} \end{bmatrix}^{-1} \times \begin{bmatrix} -e^{ik_0 z_1} \\ 0 \\ -ik_0 e^{ik_0 z_1} \\ 0 \end{bmatrix}. \tag{B-22}$$

Once we get R, A_1, A_2 and T from equation (B-22), then we can compute the equations (B-1) to (B-3) and finally the total pressure wavefield will be found. We can use the similar method for models with more interferes

C. Velocity inversion from inverse scattering series

In the seismic inversion, sources and receivers are usually deployed on the surface. For simplicity, we can set $z_g = z_0 = 0$ and define some helpful notations (similar to those by Weglein,2003Schlottmann (2006, 36)):

$$\left(\boldsymbol{G}_0\boldsymbol{V}\boldsymbol{G}_0\right)_{RS} = \frac{\omega^2}{c_0^2}\int_{-\infty}^{\infty} dz' G_0\left(0,\omega;z'\right)V\left(z'\right)G_0\left(z',\omega;0\right), \tag{C-1}$$

$$\left(\boldsymbol{G}_0\boldsymbol{V}\boldsymbol{G}_0\boldsymbol{V}\boldsymbol{G}\right)_{RS} = \frac{\omega^4}{c_0^4}\int_{-\infty}^{\infty} dz' \int_{-\infty}^{\infty} dz'' G_0\left(0,\omega;z'\right)V\left(z'\right)G_0\left(z',\omega;z''\right)V\left(z''\right)G(z'',\omega;0) \tag{C-2}$$

where the subscript RS indicates a given source/receiver geometry. From equation (A-1) we can get:

$$G\left(0,\omega;0\right) = G_0\left(0,\omega;0\right) + \left(\boldsymbol{G}_0\boldsymbol{V}\boldsymbol{G}_0\right)_{RS} + \left(\boldsymbol{G}_0\boldsymbol{V}\boldsymbol{G}_0\boldsymbol{V}\boldsymbol{G}\right)_{RS}, \tag{C-3}$$

where $G_0(0,\omega;0)$ is the wavefield from source to receiver in the reference model and $G(0,\omega;0)$ is the Green's function in the true model and is recorded by the receiver at surface with the source at surface.

In the 1-D case, we can calculate the Green's function G_0 in the reference model (with a constant velocity c_0) between two arbitrary points z_1 and z_2:

$$G_0\left(z_1,\omega;z_2\right) = \frac{ic_0}{2\omega}e^{i\omega|z_1-z_2|/c_0}. \tag{C-4}$$

Using equation (C-4) and $V(z<0)=0$, we can rewrite equation (C-1) as

$$\left(\boldsymbol{G}_0\boldsymbol{V}\boldsymbol{G}_0\right)_{RS}=\frac{\omega^2}{c_0{}^2}\int_0^{\infty}dz\left(\frac{ic_0}{2\omega}\right)^2 V\left(z\right)e^{\frac{2i\omega|z|}{c_0}}. \tag{C-5}$$

To invert $V(z)$, we can apply the inverse Fourier transform on equation (C-5):

$$V\left(z\right)=-\frac{4}{\pi c_0}\int_{-\infty}^{\infty}d\omega e^{-\frac{2i\omega|z|}{c_0}}\left(\boldsymbol{G}_0\boldsymbol{V}\boldsymbol{G}_0\right)_{RS}. \tag{C-6}$$

Assuming the source signal is a Dirac delta function, the data residual between the recorded data and the modeled data in the reference model can be represented as:

$$D_0^{resi}\left(\omega\right)=G\left(0,\omega,0\right)-G_0\left(0,\omega,0\right). \tag{C-7}$$

We can convert the data residual into a reflectivity image update using the depth migration in the reference medium:

$$U\left(z\right)=-\frac{4}{\pi c_0}\int_{-\infty}^{\infty}d\omega e^{-\frac{2i\omega|z|}{c_0}}D_0^{resi}\left(\omega\right). \tag{C-8}$$

According to equations (C-6) and (C-8), we can apply the inverse Fourier transform and rearrange the equation (C-3) as:

$$V\left(z\right)=U\left(z\right)+\frac{4}{\pi c_0}\int_{-\infty}^{\infty}d\omega e^{-\frac{2i\omega|z|}{c_0}}(\boldsymbol{G}_0\boldsymbol{V}\boldsymbol{G}_0\boldsymbol{V}\boldsymbol{G})_{RS}. \tag{C-9}$$

In equation (C-9), $V(z)$ is the variable we want to obtain. However, equation (C-9) is implicit. We can iteratively solve $V(z)$ as follows:

$$V_1(z) = U(z), \tag{C-10}$$

$$V_2(z) = U(z) + \frac{4}{\pi c_0}\int_{-\infty}^{\infty} d\omega e^{-\frac{2i\omega|z|}{c_0}} (\boldsymbol{G}_0\boldsymbol{V}_1\boldsymbol{G}_0\boldsymbol{V}_1\boldsymbol{G}_1)_{RS}, \tag{C-11}$$

$$V_n(z) = U(z) + \frac{4}{\pi c_0}\int_{-\infty}^{\infty} d\omega e^{-\frac{2i\omega|z|}{c_0}} (\boldsymbol{G}_0\boldsymbol{V}_{n-1}\boldsymbol{G}_0\boldsymbol{V}_{n-1}\boldsymbol{G}_{n-1})_{RS}, \tag{C-12}$$

where $V_n(z)$ is the perturbation after *n-th* iteration; $\boldsymbol{G}_{n-1}$ indicates the Green's function in a medium with perturbation $V_{n-1}(z)$.

Herein, to further simplify the calculation of equation (C-12), we can again utilize the equation(C-1):

$$\begin{aligned}\frac{4}{\pi c_0}\int_{-\infty}^{\infty} d\omega e^{-\frac{2i\omega|z|}{c_0}} \left(\boldsymbol{G}_0\boldsymbol{V}_{n-1}\boldsymbol{G}_0\boldsymbol{V}_{n-1}\boldsymbol{G}_{n-1}\right)_{RS} &= \frac{4}{\pi c_0}\int_{-\infty}^{\infty} d\omega e^{-\frac{2i\omega|z|}{c_0}} \left[G_{n-1}(0,\omega,0) - G_0(0,\omega,0)\right] \\ -\frac{4}{\pi c_0}\int_{-\infty}^{\infty} d\omega e^{-\frac{2i\omega|z|}{c_0}} \left(\boldsymbol{G}_0\boldsymbol{V}_{n-1}\boldsymbol{G}_0\right)_{RS} &= -U_{(n-1)}(z) + V_{(n-1)}(z),\end{aligned} \tag{C-13}$$

where

$$U_{n-1}(z) = -\frac{4}{\pi c_0}\int_{-\infty}^{\infty} \mathrm{d}\omega e^{-\frac{2i\omega z}{c_0}} D_{n-1}^{resi}(\omega), \tag{C-14}$$

$$V_{n-1}(z) = -\frac{4}{\pi c_0}\int_{-\infty}^{\infty} d\omega e^{-\frac{2i\omega|z|}{c_0}} \left(\boldsymbol{G}_0 \boldsymbol{V}_{n-1} \boldsymbol{G}_0\right)_{RS}, \tag{C-15}$$

$$D_{n-1}^{resi}(\omega) = G_{n-1}(0,\omega,0) - G_0(0,\omega,0). \tag{C-16}$$

$U_{n-1}(z)$ is the migration of data residuals $D_{n-1}^{resi}(\omega)$ between the *(n-1)-th* iteration modeled data and the recoded data in the reference velocity. $V_{n-1}(z)$ is the *(n-1)-th* iterated perturbation.

Inserting equation (C-13) into equation (C-12), we can obtain

$$V_n(z) = U(z) - U_{n-1}(z) + V_{n-1}(z). \tag{C-17}$$

Consequently, we can summary the iterative solution of perturbation $V(z)$ as follows:

Initialization:

Giving a reference median c_0;

Calculating the data residual D_0^{resi} between the observed data and the modeled data in the reference medium (equation (C-7));

Calculating the initial perturbation $V_1 = U$ by migrating the data residual D_0^{resi} (equation (C-8)).

For the n-th iteration:

Calculate the G_{n-1} based on the previous perturbation V_{n-1};

Calculating the data residual D_{n-1}^{resi} between G_{n-1} and G_0;

Calculating the $U_{n-1}$by migrating D_{n-1}^{resi} (equation (C-14));

Updating the V_n based on U, U_{n-1} and V_{n-1} (equation (C-17)).

Copy

Roya Eftekhar

May 2018